

# **Design of a Carbon Fiber Bicycle Stem Using an Internal Bladder and Resin Transfer Molding**

by

**MAXIME THOUIN**

Composite Materials Group  
Department of Mechanical Engineering  
McGill University, Montreal



A Thesis Submitted to the Faculty of Graduate Studies and  
Research in Partial Fulfillment of the Requirements of the Degree  
of Master of Engineering

© Maxime Thouin 2004



Library and  
Archives Canada

Bibliothèque et  
Archives Canada

Published Heritage  
Branch

Direction du  
Patrimoine de l'édition

395 Wellington Street  
Ottawa ON K1A 0N4  
Canada

395, rue Wellington  
Ottawa ON K1A 0N4  
Canada

*Your file    Votre référence*

*ISBN: 0-494-06590-7*

*Our file    Notre référence*

*ISBN: 0-494-06590-7*

#### NOTICE:

The author has granted a non-exclusive license allowing Library and Archives Canada to reproduce, publish, archive, preserve, conserve, communicate to the public by telecommunication or on the Internet, loan, distribute and sell theses worldwide, for commercial or non-commercial purposes, in microform, paper, electronic and/or any other formats.

The author retains copyright ownership and moral rights in this thesis. Neither the thesis nor substantial extracts from it may be printed or otherwise reproduced without the author's permission.

#### AVIS:

L'auteur a accordé une licence non exclusive permettant à la Bibliothèque et Archives Canada de reproduire, publier, archiver, sauvegarder, conserver, transmettre au public par télécommunication ou par l'Internet, prêter, distribuer et vendre des thèses partout dans le monde, à des fins commerciales ou autres, sur support microforme, papier, électronique et/ou autres formats.

L'auteur conserve la propriété du droit d'auteur et des droits moraux qui protègent cette thèse. Ni la thèse ni des extraits substantiels de celle-ci ne doivent être imprimés ou autrement reproduits sans son autorisation.

---

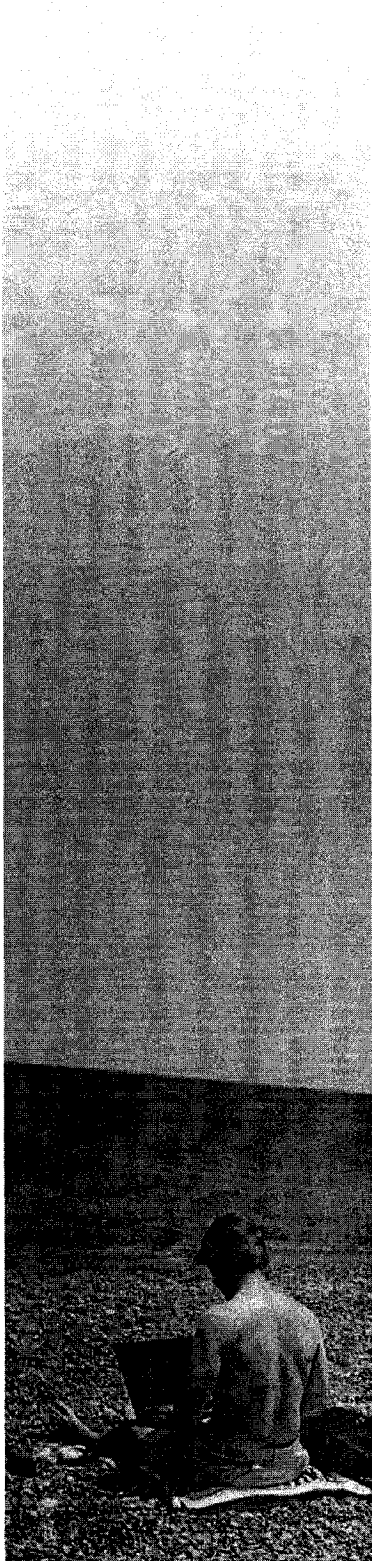
In compliance with the Canadian Privacy Act some supporting forms may have been removed from this thesis.

Conformément à la loi canadienne sur la protection de la vie privée, quelques formulaires secondaires ont été enlevés de cette thèse.

While these forms may be included in the document page count, their removal does not represent any loss of content from the thesis.

Bien que ces formulaires aient inclus dans la pagination, il n'y aura aucun contenu manquant.

  
**Canada**



*To Florent Forget, my grandfather (1918-1985).  
You motivated my curiosity from the very beginning.  
You were always there, I know.*

## **ABSTRACT**

The goal of this research is to design, analyze and manufacture a carbon fiber bicycle stem that maximizes the use of carbon fiber composites. The stem is the part of the bicycle that connects the handlebar to the fork. The design is difficult due to the small size and complex geometry of the part, thus not obvious to conceive with a standard composite manufacturing approach.

With all the required specifications and the experience of the early prototypes, a general manufacturing plan was devised. Work began with a concurrent design and analysis process. The machining and preparation of the prototyping molds followed. After a limited production of prototypes, a set of jigs was designed to perform the post-machining operations and a series of tests was run to detect any possible flaws in the design. The resulting design was successful in terms of weight, stiffness, strength and aesthetic properties.

Even though the process is here applied to a composite part for the sports industry, the manufacturing techniques developed in this project can be applied to many other fields such as aerospace or automotive.

**KEYWORDS:** bicycle stem, RTM, design, carbon braid, inner bladder, manufacturing



## RÉSUMÉ

Le but de cette recherche est de faire la conception, l'analyse et la production d'une potence de vélo qui maximise l'utilisation de la fibre de carbone. La potence est la partie qui relie le guidon à la fourche. Le projet représente un défi puisque la pièce est petite et possède une géométrie complexe, ce qui empêche l'utilisation des techniques de production traditionnelles.

Avec l'expérience acquise des prototypes antérieurs et une liste de caractéristiques bien précises, un plan de production a pu être élaboré. Tout a commencé avec une approche simultanée de la conception et de l'analyse structurelle. L'usinage et la préparation des moules ont suivi. Après une production de prototypes limitée, un ensemble de gabarits pour faciliter les opérations de post-injection était de mise. Le produit final fut un succès, autant au niveau de la structure, du poids, de la rigidité et de l'esthétique.

Même s'ils sont ici appliqués aux articles de sports, les procédés élaborés dans cet ouvrage peuvent être utilisés pour différentes applications comme l'aérospatiale et l'automobile.

**MOTS CLÉS :** potence, vélo, conception, tresse, carbone, vessie gonflable, production, moulage par transfert de résine.

## ACKNOWLEDGEMENTS

First, I would like to thank **Professor Larry Lessard** for giving me the opportunity of mastering in a subject that I am truly passionate about. He has been a great mentor and an invaluable friend. Thanks to everybody in the research group who made this possible:

- My university accomplice, **Eric St-Amant** for his great common sense and his machining abilities, which made this project a successful one.
- **Nicolas Verzeni** for his dedication to the project and great ideas.
- **Professor Pascal Hubert**, for his support and expertise.
- **Julien Bouchez, Frederic Gosselin and Ana Teodonescu** for their respective research and simulations.
- **Marc-André Oceau** for introducing me to the world of composite materials.
- **Mathieu Dakowski** for the design and manufacture of the original carbon stem prototype.
- **Martin Zahoruyko and Mike McGrath** for their hard polishing work.

I would also like to thank **True Temper Sports** for their financial support and more particularly **Graeme Horwood and Neal Haas**, for their availability and precious advices.

Finalement, je voudrais dire merci à ma mère, **Sylvie**, à mon père, **Jean**, et à ma grand-mère, **Françoise**, pour leur support, autant moral que financier. Leurs encouragements à poursuivre mes rêves et mes buts m'ont permis d'aller au bout de moi-même.

À tous, Merci.

# TABLE OF CONTENTS

<b>ABSTRACT.....</b>	<b>3</b>
<b>RÉSUMÉ .....</b>	<b>4</b>
<b>ACKNOWLEDGEMENTS .....</b>	<b>5</b>
<b>1. INTRODUCTION.....</b>	<b>11</b>
1.1 DESCRIPTION OF A BICYCLE STEM.....	13
1.2 COMPOSITE MATERIALS .....	18
<b>2. STEM DESIGN.....</b>	<b>28</b>
2.1 GENERAL DIMENSIONS .....	28
2.2 CAD MODEL .....	29
2.3 DESIGN OF MANUFACTURING .....	30
<b>3. STRUCTURAL ANALYSIS.....</b>	<b>33</b>
3.1 MATERIAL CHARACTERIZATION .....	33
3.2 MODEL DEVELOPMENT.....	35
3.3 FEA RESULTS.....	38
<b>4. MOLD DESIGN.....</b>	<b>40</b>
4.1 MOLDED INSERTS .....	41
4.2 THE EXTERNAL CAP .....	43
4.3 THE INTERNAL CAP .....	44
4.4 STEM BODY MOLD AND BLADDER HOLDER .....	49
4.5 MOLD MACHINING AND FINISHING.....	56
<b>5. INJECTIONS .....</b>	<b>58</b>
5.1 RESIN SELECTION .....	58
5.2 INJECTION PARAMETERS.....	62
5.3 RECURRING DEFECTS.....	66

<b>6. FLOW SIMULATION .....</b>	<b>69</b>
6.1 PERMEABILITY MEASUREMENTS .....	71
6.2 MODEL DEVELOPMENT .....	72
6.3 SIMULATION RESULTS .....	75
<b>7. POST MACHINING FIXTURES .....</b>	<b>78</b>
<b>8. TESTING.....</b>	<b>81</b>
8.1 TESTING METHODS .....	81
8.2 TEST APPARATUS.....	82
8.3 TEST CASES .....	86
8.4 TESTED SPECIMENS.....	88
8.5 STATIC TEST RESULTS .....	89
8.6 FATIGUE TESTS RESULTS.....	94
<b>9. CONCLUSIONS .....</b>	<b>100</b>
<b>10. REFERENCES.....</b>	<b>102</b>

## LIST OF FIGURES

FIGURE 1: LANCE ARMSTRONG ON HIS COMPOSITE BIKE [3].....	12
FIGURE 2: IDENTIFICATION OF THE BICYCLE STEM AND RELATED COMPONENTS [10] ..	13
FIGURE 3: THE THREADED FORK HEADSET [11] AND THE “7” SHAPED STEM.....	14
FIGURE 4: THE THREADLESS FORK-STEM CONFIGURATION [13].....	15
FIGURE 5: DIFFERENT STEM DESIGNS AVAILABLE ON THE MARKET. [14,15,16].....	16
FIGURE 6: TYPICAL STEM ANATOMY.....	16
FIGURE 7: SCHEMATIC OF THE RTM PROCESS .....	21
FIGURE 8: THE COMBINED BLADDER-RTM PROCESS [42] .....	25
FIGURE 9: THE SAME BRAID, SHOWN FOR TWO DIFFERENT DIAMETERS REVEALING CHANGES IN FIBER ANGLE .....	26
FIGURE 10: GENERAL DIMENSIONS AND DESIGN OF THE STEM .....	28
FIGURE 11: PARAMETERIZATION CURVES USED IN THE CAD MODEL .....	29

FIGURE 12: THE STEM INSERTS .....	31
FIGURE 13: THE TWO FOLDED SECTIONS CONNECTING THE INSERTS .....	32
FIGURE 14: THE STANDARD TEST MOLD, PICTURE FRAME AND SAMPLE COUPONS .....	33
FIGURE 15: STRESS-STRAIN CURVE AND LINEAR INTERPRETATION FOR BRAIDED FABRIC AT 30° .....	34
FIGURE 16: STRESS-STRAIN CURVE AND LINEAR INTERPRETATION FOR BRAIDED FABRIC AT 45° .....	34
FIGURE 17: STRESS-STRAIN CURVE AND LINEAR INTERPRETATION FOR BRAIDED FABRIC AT 60° .....	34
FIGURE 18: THE FEA MODEL HIGHLIGHTING THE DIFFERENT MATERIAL SECTIONS.....	36
FIGURE 19: THE CLAMPING LOADS SIMULATION CASES .....	37
FIGURE 20: THE MODELS FOR RIDING LOADS AND FULL STEM ANALYSIS .....	37
FIGURE 21: THE FEA RESULTS UNDER SERVICE LOADING DEPICTING FAILURE INDEX IN PLY #1 .....	39
FIGURE 22: THE POLYURETHANE INSERTS MOLDS. ....	42
FIGURE 23: THE EXTERNAL CAP TRIM LINE .....	43
FIGURE 24: THE EXTERNAL CAP TOOL .....	44
FIGURE 25: THE CUSTOM-MADE ALUMINUM INSERT AND THE INTERNAL CAP .....	46
FIGURE 26: THE POSITION OF THE CUSTOM INSERTS IN THE MOLD .....	46
FIGURE 27: THE INTERNAL CAP MOLD AND EJECTOR DEVICES .....	47
FIGURE 28: THE DESIGN OF AN EJECTOR SCREW SYSTEM .....	48
FIGURE 29: THE MOLD USED TO MAKE THE BLADDER DIPPING MANDRELS.....	50
FIGURE 30: THE TEN FINISHED BLADDER-DIPPING MANDRELS. ....	50
FIGURE 31: A LATEX BLADDER SAMPLE .....	51
FIGURE 32: THE PRE-FORMING PROCESS .....	52
FIGURE 33: EXPLODED SCHEMATIC OF THE BLADDER HOLDER SYSTEM.....	53
FIGURE 34: ASSEMBLY OF THE BLADDER HOLDER .....	54
FIGURE 35: THE STEM MOLDING AND GENERAL GEOMETRY OF THE MOLDS.....	55
FIGURE 36: THE ALIGNMENT SYSTEM FOR THE CARBON STEERER TUBE INSERT .....	55
FIGURE 37: EXTERNAL CAP MOLD ON THE CNC AND SCALLOPS LEFT IN THE STEM MOLD AFTER MACHINING .....	57

FIGURE 38: THE FINISHED STEM BODY MOLDS .....	57
FIGURE 39: LOCATION OF THE RECURRING DRY PATCH .....	66
FIGURE 40: VOIDS IN THE HANDLEBAR FACE OF THE STEM .....	67
FIGURE 41: PROBLEMATIC REGION ON THE HANDLEBAR MOUTH .....	68
FIGURE 42: PERMEABILITY OF BRAIDED FABRICS AS A FUNCTION OF VOLUME FRACTION .....	72
FIGURE 43: THE TWO FLOW SIMULATION MODELS .....	73
FIGURE 44: HIGH PERMEABILITY FLASH SIMULATIONS .....	75
FIGURE 45: FILLING OF THE MOLD WITH REGION OF HIGHER PERMEABILITY.....	76
FIGURE 46: HANDLEBAR FILLING SIMULATION SHOWING POSSIBLE AIR ENTRAPMENT REGION.....	77
FIGURE 47: THE ROUGH AND FINISHED STEMS .....	78
FIGURE 48: THE STEM POST-MACHINING FIXTURE .....	79
FIGURE 49: ROUTING EXTRA MATERIAL ON THE STEM USING TEMPLATES .....	80
FIGURE 50: THE TEST EQUIPMENT.....	82
FIGURE 51: THE TORSION TEST FIXTURE .....	83
FIGURE 52: SIMPLE CASE OF CLAMPED END TORSION.....	83
FIGURE 53: THE BENDING TEST FIXTURE .....	84
FIGURE 54: SIMPLE CASE OF CLAMPED BEAM UNDER BENDING LOAD .....	85
FIGURE 55: STATIC TORSION TEST - EXAMPLE OF PLOTTED RESULTS .....	90
FIGURE 56: STATIC BENDING TEST - EXAMPLE OF PLOTTED RESULTS .....	91
FIGURE 57: FATIGUE TORSION TEST - EXAMPLE OF PLOTTED RESULTS .....	95
FIGURE 58: BENDING FATIGUE FAILURE RESULTS OF STEM T3.....	96
FIGURE 59: BENDING FATIGUE OF SAMPLE T4 .....	97
FIGURE 60: NORMALIZED RESIDUAL STIFFNESS OF A UNIDIRECTIONAL 0° PLY UNDER LONGITUDINAL TENSILE FATIGUE LOADING CONDITIONS [101].....	98
FIGURE 61: THE FINAL PRODUCT .....	101

## LIST OF TABLES

TABLE 1: AVAILABLE COMPETITIVE PRODUCTS .....	17
TABLE 2: PROPERTIES OF THE TWO BRAIDED TUBES GEOMETRY .....	30
TABLE 3: RESIN SYSTEMS EVALUATED .....	59
TABLE 4: IMPORTANT RESIN PROPERTIES .....	60
TABLE 5: PROPERTIES OF THE DIFFERENT ZONES OF THE STEM SIMULATION.....	73
TABLE 6: INITIAL MATERIAL PROPERTIES .....	74
TABLE 7: TESTED STEMS.....	88
TABLE 8: STATIC TESTS RESULTS FOR THE DIFFERENT DESIGN ITERATIONS .....	92
TABLE 9: STIFFNESS PROPERTIES OF COMPETITIVE PRODUCTS COMPARED WITH THE FINAL DESIGN ITERATION .....	93
TABLE 10: FATIGUE TESTS RESULTS .....	97

## LIST OF EQUATIONS

EQUATION 1: THE CHANGE IN DIAMETER OF A BRAIDED TUBE .....	26
EQUATION 2: MAXIMIZING THE EJECTOR SCREW TRAVEL .....	48
EQUATION 3: DARCY'S LAW.....	70
EQUATION 4: EVALUATION OF EMPTY CHANNEL PERMEABILITY .....	74
EQUATION 5: TORSIONAL STIFFNESS OF CLAMPED END TORSION .....	83
EQUATION 6: BENDING STIFFNESS OF CLAMPED BEAM UNDER BENDING LOAD .....	85

# 1. INTRODUCTION

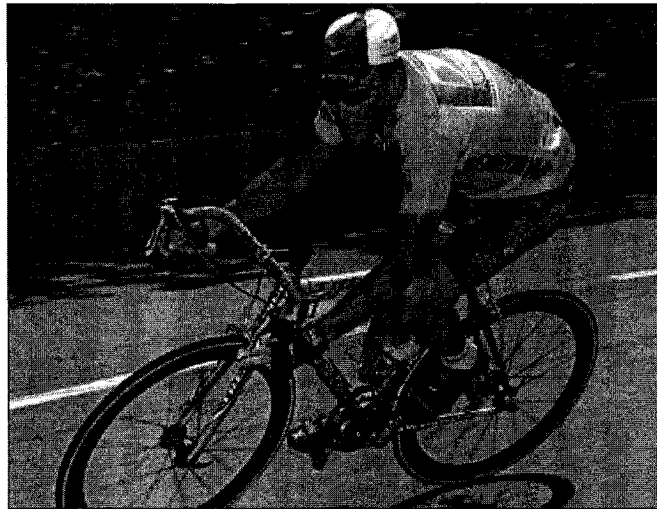
Within the last twenty years, fiber reinforced parts have played a major role in the improvement of sports equipment. Their stiffness, lightweight and appealing appearance have made them a must in all performance sports. In many disciplines such as hockey, tennis and fishing, composites are progressively replacing the traditional wood equipment. Of course, weight saving has been the major driver for such changes. However, design optimization driven by the study of load applications has been a major contributor to performance enhancement [1,2]. Moreover, the inherent damping properties of carbon fiber composites and their proven durability also played a major role in this market reorientation [3].

Traditionally, composites have been used almost exclusively in aerospace, which normally does not need to produce parts in large quantity. The new demand for composite products has pushed the sports equipment manufacturers to develop new, high volume manufacturing methods to meet to the consumer demand [3,4]. In 1990, already 10 percent of the fiber produced worldwide was used for sport equipment end recreation application. Sport is the third largest user of advanced composites behind defense/aerospace and elastomer reinforcement [5].

The cycling industry has played major role in the development of new manufacturing processes to improve the performance of bicycles by reducing weight and improving properties. As an example, champions such as Greg Lemond and Lance Armstrong have won the Tour de France on bicycles almost exclusively made of carbon fiber (Figure 1) [3]. "Composites lend themselves to a range of possible frame designs because they are not limited by the inherent material properties of metals", says Jim Colgrove, head of Trek's OCLV carbon engineering group [6]. Since then, a large number of graphite parts have flooded the market such as forks, handlebars and seat posts. In a paper published in 1993, Stephen C. Levin had predicted this diversification of the bicycle market through the use of composite materials



[7]. His report stated that bicycle components had the best potential to generate profit since they showed higher profit margins than complete bikes or frames and because riders will tend to upgrade their bikes while keeping the same frame.



**Figure 1: Lance Armstrong on his composite bike [3]**

However, prior to 2003, no manufacturer could produce a handlebar stem entirely made of composite materials. The stem is the part that connects the handlebar to the steerer tube of the fork (see Figure 2). This void in the market is somewhat surprising since the stem is an important component that is subjected to high loading. Typically, racers will use their arms on the handlebars to counteract the high loads imparted to the pedals, creating an impressive amount of torque on the stem [8,9]. The stem should also be stiff enough so that it has minimal deflection when the rider leans on it. Furthermore, as it is responsible for the control of the bicycle, failure of the stem must be avoided.

This research encompasses the design, manufacturing and testing of a new prototype bicycle stem that maximizes the use of carbon fiber over metallic inserts. In order to be competitive in the market, the target weight was set below 125 grams. The major design challenge resides in the small

size of the part and the rapid manufacturing of a strong hollow component. The stem body should also be molded so it requires no further bonding. This is why the post-molding operations are also an important issue. Fixtures must be designed in order to obtain reproducible parts. This research will cover the complete design process, beginning with a simultaneous modeling (CAD) and finite element stress analysis (FEA). All aspects of prototype development will then be described, such as mold design, flow modeling and manufacturing parameters, and concluding with the testing of the prototypes. However, before going into the design, it is important to clarify the different concepts referred to in this research.

## 1.1 Description of a Bicycle Stem

The stem connects the handlebar to the fork. It is an important component of the bicycle geometry that contributes to the ease of handling as well as the position and comfort of the rider. Since it is connected to the steerer tube, a description of the stem is impossible without first inspecting the different stem-to-steerer tube connection methods available on the market. These connections are commonly named *headsets*.

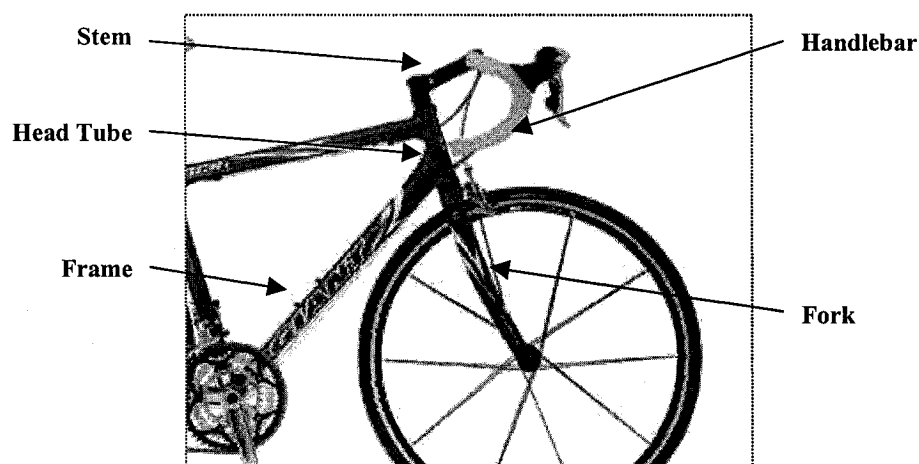
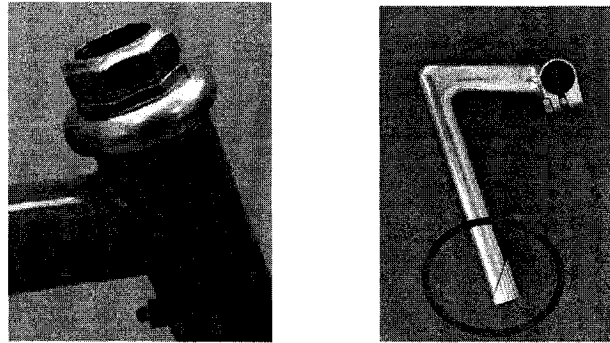


Figure 2: Identification of the bicycle stem and related components [10]

### *The headset configurations and respective stem designs*

The fork attachment to the body generally comes in two different designs: threaded and threadless steerer tubes. The first one is the classic one. A bearing race is press-fitted on the fork crown (junction of the tube and the branches) while bearing cups are pressed into the bike head tube. The top most bearing race and the steerer tube are threaded to fit each other and adjust the tension applied on the bearings. A lock nut is then installed over the connection to fix the assembly.



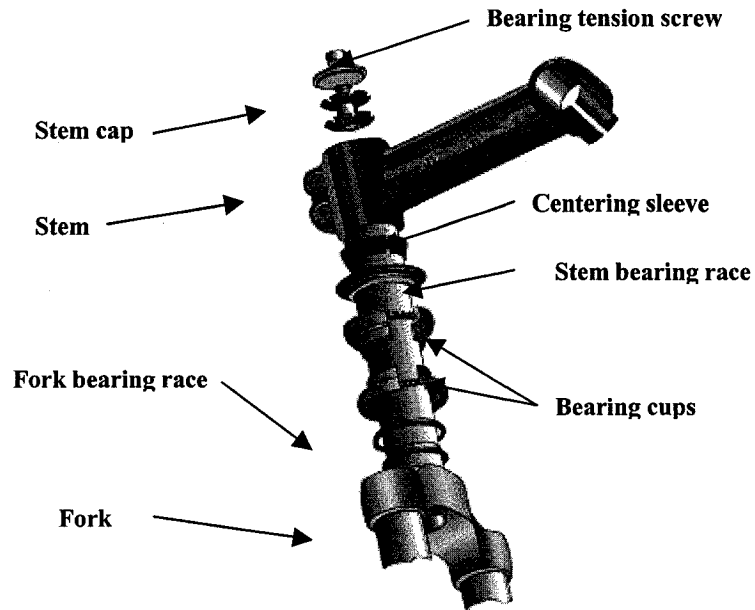
**Figure 3: The threaded fork headset [11] and the “7” shaped stem.**

Note the wedging mechanism used to fix the stem in the steerer tube (circled)

A “7” shaped stem is inserted in the steerer tube, left open at the top. The stem uses a wedging system, commonly made of an angled nut at the end of a long screw (see Figure 3), to remain in place. This design is becoming less popular since it tends to damage the steerer tube by applying non-uniform loading. The only people still using this design do it for sake of tradition.

The most common current design is the threadless headset, also called aheadset [12], the brand name under which the system is patented. Similar to the threaded one, the fork is rotating inside two sets of pressed cups and races. However, in this arrangement, the steerer tube goes

all the way through the bike head tube. As shown in Figure 4, a cap is placed on top of the stem to apply pressure on the bearings and fix the whole assembly.

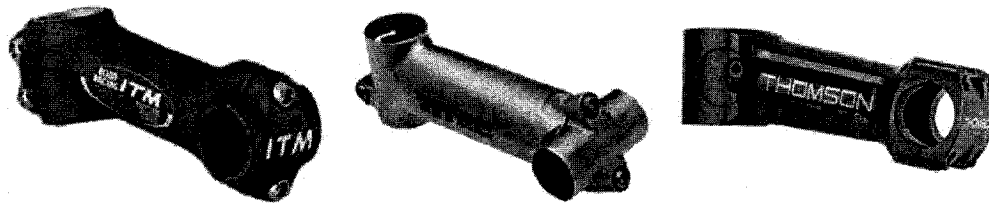


**Figure 4: The threadless fork-stem configuration [13]**

The stems used for this type of configuration are basically made of two clamps, a vertical one for the steerer tube and a horizontal one for the handlebar. Therefore, since this layout is more popular and much lighter than the threaded one, the stem was designed to fit a threadless tube. This design also has a much better potential for composite integration, since the wedging mechanism would be incompatible with a carbon fiber fork tube.

#### Current market review

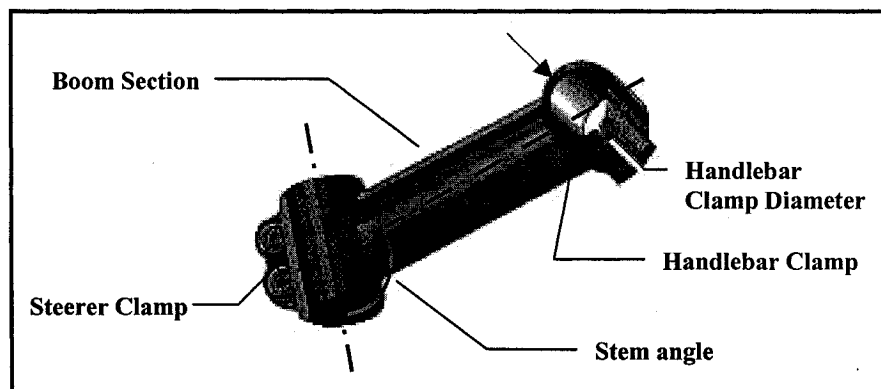
There are several existing stem designs. Most of them are made of metallic alloys such as steel, aluminum or even magnesium. As seen in Figure 5, their shapes, sizes and fastening methods are extremely diversified.




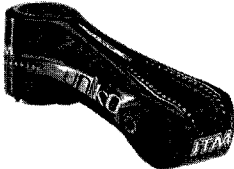



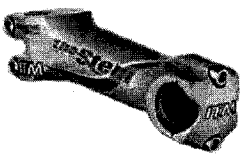
**Figure 5: Different stem designs available on the market. [14,15,16]**

The new prototype falls into the high-end market. It was therefore important to target its competitive products for comparative purposes. Table 1 shows the different stems that were identified as benchmarks for the design.

It is evident from Table 1 that this is not the first stem design to incorporate the use of carbon fibers. However in every case, the designers relied on aluminum for the clamping devices and used carbon fiber in the boom section of the stem (see Figure 6). This is where the current research differs from the competition, by reducing the amount of metal content to a minimum.



**Figure 6: Typical Stem Anatomy**

Picture	Manufacturer and Model	Material	Weight (g)	Clamp Diameter (mm)	Angle (degrees)
	Time Monolink [17]	Carbon with metallic skeleton	135	31.8	80 / 100
	ITM Uniko [14]	Carbon	155	25.8	80 / 100
	3ttt More [18]	Carbon	170*	31.8	80 / 100
	Deda Forza [19]	Carbon	119	31.8	82 / 98
	Deda Mag 00 [19]	Magnesium	112	31.8	82 / 98
	ITM The Stem [14]	Magnesium	95	25.8	80 / 100

\* Weight given for the 110mm instead of the standard 120mm

**Table 1: Available competitive products**

## 1.2 Composite Materials

### Definition

A composite material consists of an heterogeneous assemblage of two materials of different nature, completing each other and leading to a material where the performance is greater than that of the components taken separately [20]. Nowadays, most composite materials for high performance structural elements are made of a combination of synthetic fibers and polymer resin. The reinforcement (fibers) gives the strength to the parts while the matrix (resin) maintains the integrity of the part.

### Manufacturing processes overview

There are several ways to manufacture composite parts. The selection of the process depends mostly on the geometry and the end use of the design. A definite advantage of composite materials is their oriented properties. Unlike isotropic materials, the properties of a composite (orthotropic) material depend on the orientation of the reinforcements. It allows *tailoring* of the composite in order to remove material in areas and directions where stress is minimal [21]. The selected process should be able to comply with the required arrangement of the fibers. Moreover, the selection of manufacturing technique has an impact on the production time and cost, mechanical properties, fiber volume fraction and surface finish. The designer's work is to evaluate the pros and cons of each applicable method and choose the one that is believed to give the best results. Some of the most commonly used methods are presented below with a short description.

- **Hand / Wet Lay-up:** The dry fibers are placed in a mold surface and painted with resin.

- **Pultrusion:** Impregnated fibers are mechanically pulled through a die.
- **Filament Winding:** A rotating mandrel is mechanically wrapped with continuous impregnated fiber reinforcement.
- **Infusion:** A dry fiber pre-form is placed in a vacuum bag. Resin is then drawn through the pre-form. This method is often used to produce large parts.
- **Prepreg and Resin Transfer Molding** are the two most widely used techniques to make high performance composite parts. A more in-depth evaluation of both methods is pre-formed in order to choose the appropriate one for this application.

#### *Pre-impregnated fabric and tapes (Prepreg)*

Prepreg is an abbreviation for (fibers) *pre-impregnated* (with resin). In this process, the fibers are coated with resin as they are woven or rolled in unidirectional tape. Heat is used to polymerize the resin and solidify the part. Prepregs are widely used in several advanced composite designs due to their precise control over fiber volume ( $V_f$ ) ratio and precise layer cutting possibilities. Moreover, prepreg design works with a wide variety of tooling systems. The material and cost of the mold depend on the complexity and number of parts that need to be produced. A common way to process prepregs is to place the fiber lay-up on a mold surface and cover it with a hermetic (vacuum) bag. Since the fiber layers are tacky, it is relatively easy to stack the different layers on top of each other. To create compaction and retrieve air from the part, vacuum pressure is applied within the bag and the part is forced to comply with the mold shape. Aerospace quality parts are normally placed in autoclaves (large pressurized ovens) where the applied



pressure on the laminate will no longer be limited to atmospheric pressure. A typical autoclave has the capacity pressurize up to about 5 MPa, usually by means of pressured nitrogen [22]. This allows for a high level of part consolidation, which is known to improve physical properties. Also, voids and air bubbles are more properly squeezed out and the layers are pushed up against the mold surface, creating better dimensional tolerance on the finished part. On the negative side of prepregs, handling of these fabrics can be very difficult. In a production environment, the operator must be very careful to align the plies in accordance with designer specifications. Different systems have been developed to solve this problem such as laser positioning systems and automated tape cutting and lay-up machines.

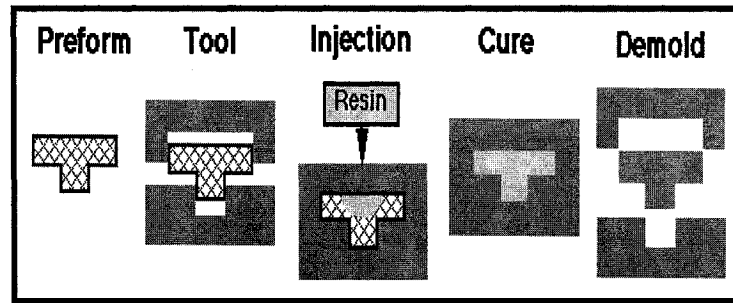
Designs that use pre-impregnated fibers have been incorporated into the sporting goods industry for many years. In 2002, recreational applications accounted for US\$38.9 millions of Hexcel's sales, a world leader in production of prepreg fabrics [1]. Companies such as GT and Kestrel build their competition monocoque bicycle frames using pre-impregnated carbon fiber [23,24]. Both these companies use an internal bladder to consolidate the material against the closed steel mold.

Although it is widely used in many different applications, the raw material has further disadvantages of being very expensive and creating a lot of waste. The waste problem can be minimized using numerically controlled cutters and optimized cutting patterns. However, the intermediate step of impregnation is still very costly. This high cost has encouraged many designers to consider alternative manufacturing methods.

### *Resin transfer molding (RTM)*

Closely related to infusion, RTM is a closed, rigid mold process. As shown in Figure 7, a dry fiber pre-form is placed between two mold surfaces and an injection pump is used to push resin through the fibers. The air exits through the strategically placed vents as the resin front advances. The

injection is stopped when all the air is evacuated from the mold. The resin can then be cured and when the cure is completed, the part is ready to be demolded. Similarly to the infusion process, it is possible to use vacuum assistance in order to reduce the air entrapment and assist resin injection [25].



**Figure 7: Schematic of the RTM process**

The science of RTM is fairly new. It only gained in popularity during the 1980's, although applications of RTM began as early as 1946 [26]. It is only with the development of low-viscosity and high performance resins that high fiber-resin ratios were achievable, which attracted more designers to consider RTM. It is now considered to be a cost effective [25,27] process that is used in many applications ranging from mass production of car spoilers [28] to specialized production of missile shrouds [29].

There are many advantages to RTM. First of all, since the tools are machined to the outer dimensions of the final part, a high level of dimensional tolerance is achievable. Excellent surface finish of the part is also attainable, which is related closely to the quality of the tool [21,30]. Thus, it is possible to produce components that require minimal post-molding finishing. It is also very flexible, since almost any type of reinforcement or resin system can be used. Buying resin and dry fiber material in bulk makes the process less expensive than prepreg by saving the intermediate step of combining them into a prepreg. It is also known to be a safer production process than hand lay-up because the operator is not in direct contact with the resin and avoids

inhaling hazardous volatiles such as styrene [31]. Moreover, very complex components can be made using RTM. Dry fabrics allow much better *drapability* (the ability to conform to the mold shape) than pre-impregnated material [32]. The possibility to mold difficult shapes means that a high level of part integration can be achieved, which leads to lower costs and faster production rates [4,21]. Incorporating several substructures together into one major structure is more efficient both structurally (structural integrity) and in terms of productivity [27]. This advantage of RTM increases reproducibility of the process and enhances quality control [4].

Compared to plastic injection molding or autoclave curing, RTM is considered a low-pressure process. It is usually performed between 1 and 10 atm although most applications will not exceed 6 atm. This means that injection can be performed using inexpensive means such as a pump powered only by pressurized air.

However, RTM has its drawbacks. The fibers can be washed away by the flow of resin and the subsequent change in fiber orientation can affect the mechanical properties of the final product [31]. Also, although some work was done to implement low-cost tooling [33], production molds are usually expensive due to the close tolerances and materials used (typically aluminum or steel). The tooling can be even more expensive when it comes to complicated parts since more time will have to be put in the design of the injection pattern and machining. The location of the injection port(s) and vent(s) is critical to a complete filling of the mold. One needs to carefully study the geometry of the part and the subsequent flow of resin through the resin in order to design an effective RTM tool. Finally, the manipulation of dry fabric sometimes makes the pre-forming and lay-up awkward. Tackifier, hot pressing and different braiding and sewing techniques were developed or adapted to facilitate these procedures [21,34]. However, when using tackifier, it is important to make sure that it is compatible with the used matrix, as shown in Berthelet et al. [35]

Just like any composite process, the success of RTM is dependent on several factors. For RTM, the critical ones are the process temperatures of the resin or the mold, the injection pressure profile, the mold design, the quality of the pre-form and operator skills [21]. Thus there are many parameters that have to be set and optimized, especially for an extended production environment.

Fiber wetting and permeability are two concepts that one has to be aware of in order to obtain a quality part. Fiber wetting describes the ability of the resin to bond with the dry fibers and has a direct effect on the quality of the final part. A good consolidation and thorough wetting of the fibers is of primary importance. This is also why permeability of the pre-form is important. Permeability is the property of a media that defines how easily fluid can flow through it. In RTM science, it is widely used to predict the resin flow front by using Darcy's law of flow through a porous media. Combining the permeability, the pressure difference and the viscosity of the resin, one can use Darcy's law combined with finite element techniques to simulate the injection process [36,37]. This allows the designer to position the mold injection ports and vents adequately in order to achieve a reliable and reproducible process. This concept will be further explained in section 6 on injection simulation of the molds.

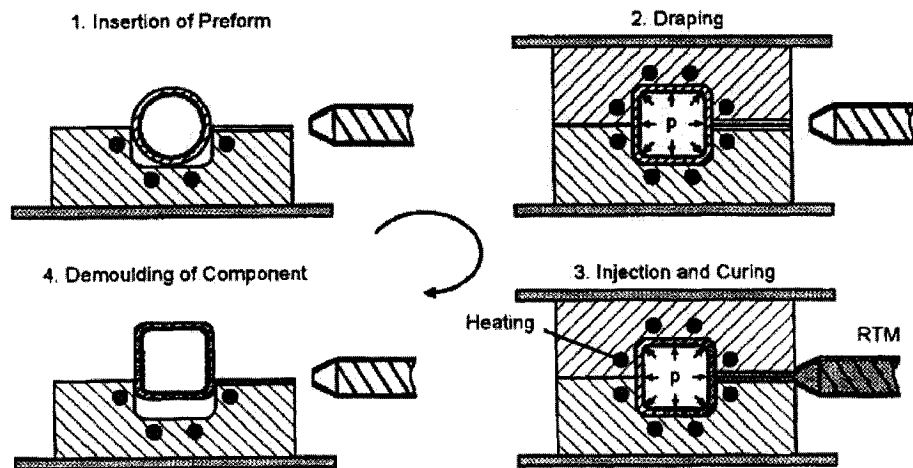
Evaluating the different advantages and difficulties of RTM in relation to the new stem prototype part, it was thought to be the process of choice. The difficult geometry of the part and the possibility for a fast production cycle made it very appealing.

Already, many different bicycle components have been developed using RTM. Namely, Oceau and Lessard [38] were successful at designing an extra-light carbon fiber fork with a titanium steerer tube. A machined foam core was used to fill the braided fabric. Similarly, Quaresimin et al. optimized the design of a carbon fiber crank set by RTM [39]. However, the proposed prototype for this research shall not make use of a foam core but will be

hollow in order to satisfy the challenging weight target. Consequently, alternative methods for making hollow parts were investigated.

### *Hollow molding using resin transfer molding*

There are several manufacturing methods used to produce hollows components. Water soluble cores, thermoplastic cast inside metal tools, filament winding and shrink tape over a metal mandrel are only a few of the possible processes already developed [40]. The decision of using an inflatable bladder was based on ease of manufacturing and because it allows for superior material consolidation. The process could also be used with prepreg fibers but the wrapping of the flexible bladder is very difficult and leaves a great margin for error. Also, the stickiness (tackiness) of the prepreps and their lower drapability restricts the possibility of conforming to small radii [32]. In the RTM process, dry fibers are loosely placed around an inflatable bladder before being inserted in the mold cavity. The bladder is then inflated and fibers become draped to the mold surface. As shown in Figure 8, the injection flows around the pressurized bladder and exits by the vent. After curing, the hollow part can then be de-molded. Depending on the type of bladder, it can either be retrieved or left inside the part. Thinner bladders can remain in the part without affecting the mechanical properties [32], as is the case with typical composite squash and tennis racquets. However, if the remaining bladder becomes loose, then it will tend to cause vibrations or rattles that may bother the user [41].



**Figure 8: The combined bladder-RTM process [42]**

One of the main advantages of bladder molding is the possible use of continuous braided fibers. Using this type of reinforcement allows the making of a 3-D hollow part without any seams or discontinuities, improving the performance of the laminate. This is especially useful for complex geometries [43]. It also facilitates the lay-up process as the bladder is simply inserted inside a tubular pre-form instead of having to wrap around it. In the production of tubular components such as baseball bats, the combination of braided sleeving and RTM has been called a “marriage made in heaven” [44]. In spite of this, braided fibers pre-forms have the particularity of changing fiber angle and thickness when the braid diameter is varied. Designers have to take these property changes into account since it directly affects the mechanical behavior of the final part [45]. The mathematical relationship between the braid diameter and the fiber angle can be described by the following equation [46].

$$l_2 = \frac{l_1 \sqrt{\left(\frac{D_1}{D_2}\right)^2 - \sin^2 \alpha_1}}{\cos \alpha_1} \quad (1.1)$$

$$\alpha_2 = \arcsin\left(\frac{D_1}{D_2} \cdot \sin \alpha_1\right) \quad (1.2)$$

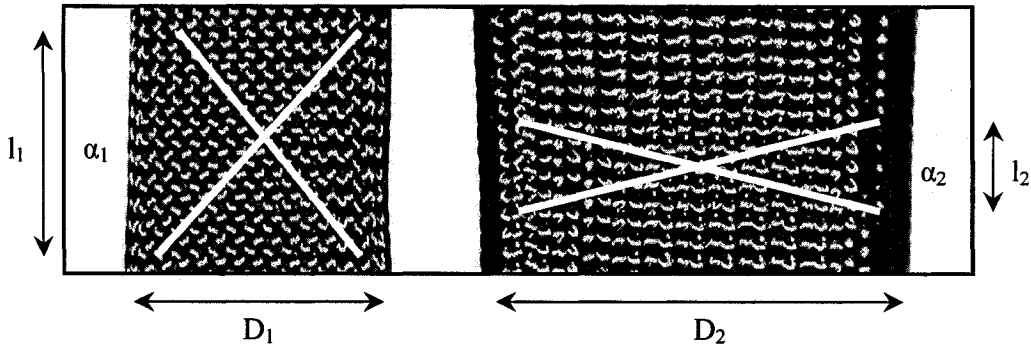
where

$l_1$  &  $l_2$  = length

$\alpha_1$  &  $\alpha_2$  = fiber angle

$D_1$  &  $D_2$  = braid diameter

**Equation 1: The change in diameter of a braided tube**



**Figure 9: The same braid, shown for two different diameters revealing changes in fiber angle**

The change in fiber angle not only affects the mechanical behavior of the final product but the way the flow travels at the moment of injection.

The change in thickness resulting from changing the braid diameter can easily be calculated by using the *braid calculator* provided by A&P technologies, on their website [47]. The change in thickness is critical when designing inserts or cores since the remaining thickness of the fibers can locally affect the fiber/resin ratio and therefore, the permeability. Eventually, this will have an impact on the resin front at the time of injection.

The combined bladder-RTM process is widely documented by Michaeli & al. in various publications [32,45,42,46,48]. The articles contain several experimental approaches for different process parameters such as draping of the fibers in different mold geometries, permeability and working pressures. Although the combined application of the RTM process and the inner bladder molding is established, it still presented a difficult design challenge when adapted to the needs of this project, considering the relatively small size of the part. Namely, the connection method of the bladder remains a challenging issue in this process. The present research explores a novel approach for the integration of a bladder holder tool within the sealed injection perimeter. Further description of the process will be provided along the presentation of the work done on this design.



## 2. STEM DESIGN

### 2.1 General Dimensions

Figure 10 shows the basic design of the stem, which is similar in dimensions and clamping method to conventional designs. The specifications of the stem were set with an industrial partner in order to be competitive in the market and fulfill consumer demand. The stem is 120 mm long and is designed to weigh less than 125 grams. The handlebar clamp was made to accommodate a 31.8 mm handlebar tube, while the steerer tube is 28.6mm in diameter. A stem angle of 82 degrees was found to be within market standards and popular with the riders.

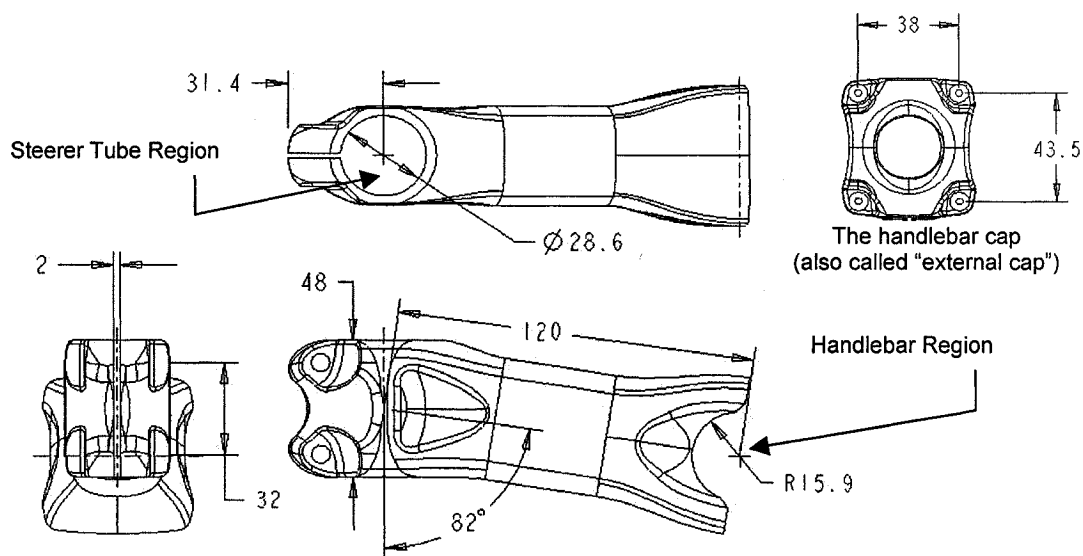


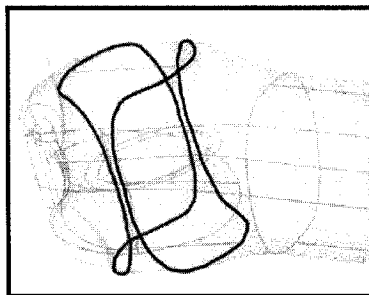
Figure 10: General dimensions and design of the stem

The steerer clamp is closed with two M5 screws that clamp around the steerer tube. To avoid metallic inserts in this area, the stem is drilled through and a special sleeve is used to fasten the screws. The flat regions where

those fasteners are located have been integrated into the stem shape to avoid machining into the fibers after the injection. This also improves the structural integrity of the part. The handlebar clamp has four threaded aluminum barrels molded within the stem to fix the cap over the bar. It uses four M4 fasteners instead of the conventional two because this configuration is judged to be safer and tends to dissipate the handlebar load over a larger surface [49]. The wide mouth of the handlebar clamp was designed to create maximum of friction on the bar, thus reducing the possibility of slipping and improves stress distributions at the bar/clamp interface.

## 2.2 CAD Model

An aesthetically attractive CAD model was obtained but not easy to achieve. Optimization of the stem from the original prototypes required removing a lot of volume in the steerer tube region. This meant that the rectangular elevation of the steerer cylinder had to merge into the circular cross section of the boom extension. It was made possible by defining three-dimensional intersection curves (Figure 11) and connecting them with blended surfaces.



**Figure 11: Parameterization curves used in the CAD model**

The red and blue lines are the discussed 3D intersection curves

The model was made in such a way that all the critical dimensions were parameterized. This becomes convenient when modifying and optimizing the stem shape and when designing the post machining fixtures

(section 7). The parametric model was also done for the future purpose of producing other similar stems in different sizes (shorter or longer).

## 2.3 Design of Manufacturing

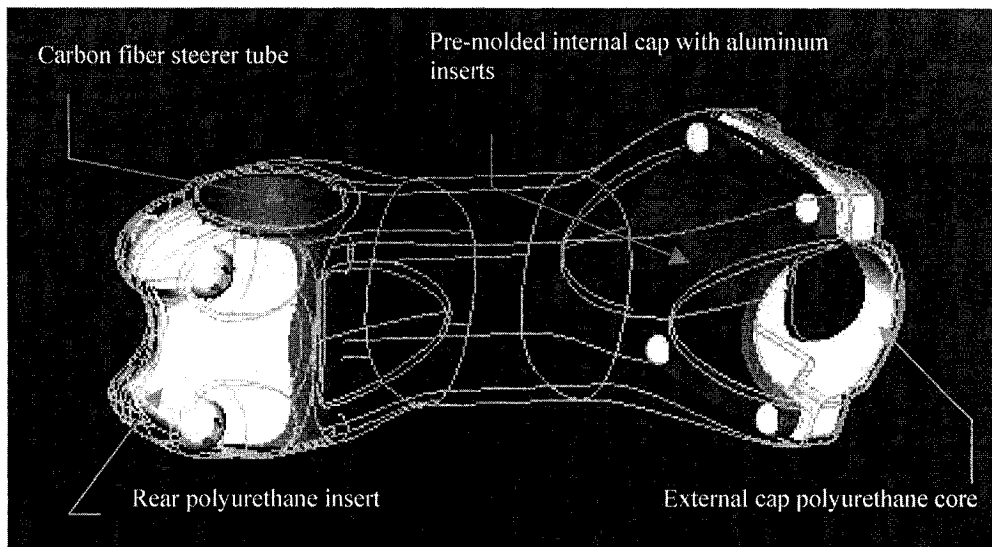
The stem body is mostly made of braided carbon fiber tube. The size has to be picked to accommodate the large change in diameter along the stem and still deliver the expected mechanical properties in critical regions. The biggest supplier of braided carbon fiber in North America is A&P Technologies. Two of their standard products were targeted as possible raw material for the building of the prototypes. Their specifications are described in Table 2 [50].

<b>A P Technology</b>				<b>GAMMASOX™ Carbon Fiber Braids</b>					
PRODUCT CODE	DIAMETER		ANGLE	YIELD		FABRIC	WEIGHT	THICKNESS at 50% FV	
	in	mm	+/-	ft/lb	m/kg	oz/yd <sup>2</sup>	g/m <sup>2</sup>	in	mm
MEDIUM FABRICS									
<b>U57L200X</b>	<b>2.00</b>	<b>50.8</b>	<b>45°</b>	<b>22.1</b>	<b>15</b>	<b>12.4</b>	<b>420</b>	<b>0.018</b>	<b>0.46</b>
<b>V57L250X</b>	<b>2.50</b>	<b>63.5</b>	<b>45°</b>	<b>18.4</b>	<b>12</b>	<b>11.9</b>	<b>403</b>	<b>0.018</b>	<b>0.46</b>
<i>Sleevings braided with 34 Msi modulus, 640 ksi tensile strength carbon.</i>									

**Table 2: Properties of the two braided tubes geometry**

The manufacturing is achieved through the use of various inserts. The first insert is the carbon steerer tube. A 26.8mm ID tube with a 1mm wall thickness is pre-made using prepreg on a mandrel. This tube is then cut to size before being inserted in the stem mold. Also, since the bladder cannot get through the steerer tube a lightweight insert has to be placed in the steerer tube region (see Figure 12). This insert is made of molded-to-shape polyurethane. This polymer is very strong in compression, has a low density and exhibits a good chemical bonding compatibility with epoxy. Using inserts

increases the thickness of certain areas without compromising the weight target. Furthermore, it provides just enough room in the mold for the fiber thickness required in order to obtain the desired fiber/resin ratio. Note that the **external cap** is also made in similar fashion.

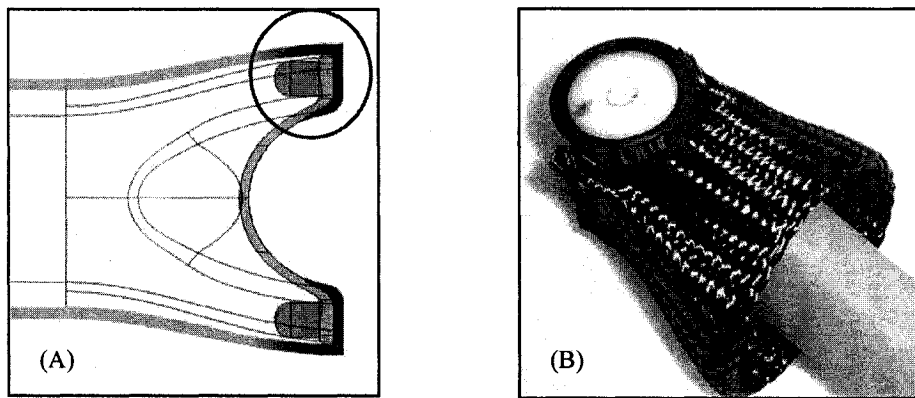


**Figure 12: The stem inserts**

Finally, another insert called the **internal cap** is placed to make the inside surface of the stem. This carbon insert is pre-molded and contains the aluminum barrels that will later be threaded. Figure 12 shows the position of each insert inside the stem. One of the major concerns in this design is the structural integrity between the skin layer and all the other inserts. This problem is one of great importance since it directly affects the reliability of the final product. To solve this issue in the handlebar area, the end of the pre-form is folded over the two flat surfaces of the internal cap (shown in Figure 13-A). This encloses the insert and keeps it from being ripped off in case of an impact. Also, the testing of early prototypes led to the implementation of another fiber overlap layer between the steerer tube insert and the body. In the original design, the tube was only joined to the skin by a thin resin bond on its ends. The implemented solution is a folded braided tube that connects

the entire exposed surface of the tube to the rest of the body. This arrangement is shown in Figure 13-B.

This shows how closely related mechanical behavior and production implementation are when using the RTM process. The design was also conducted using principles of simultaneous engineering [51] by running concurrent mechanical analysis through the process. Several numerical models and load cases were tackled in order to validate the CAD design.



**Figure 13: The two folded sections connecting the inserts**

- (A) The fiber from the pre-form is folded over the internal cap (blue region).
- (B) The carbon fiber interface between the steerer tube and the body.

### 3. STRUCTURAL ANALYSIS

#### 3.1 Material Characterization

In order to get reliable structural analysis results, it was important to characterize the material as well as possible before intending to simulate its behavior. In order to obtain the physical properties of braided carbon fiber fabric, a special mold was machined, respecting ASTM standards [52]. The mold was made to accommodate different sample thicknesses by means of a picture frame placed between the two mold faces that can have any thickness (Figure 14). The sample test specimens were injected using four plies of carbon fiber braid, which results in a test section thickness of 2 mm. The samples have thicker ends (tabs), covered with fiberglass to avoid breaking at the base and provide a firm clamping region for the grips of the test machine.

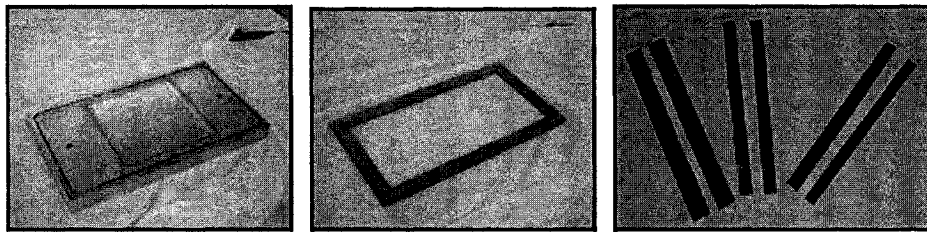
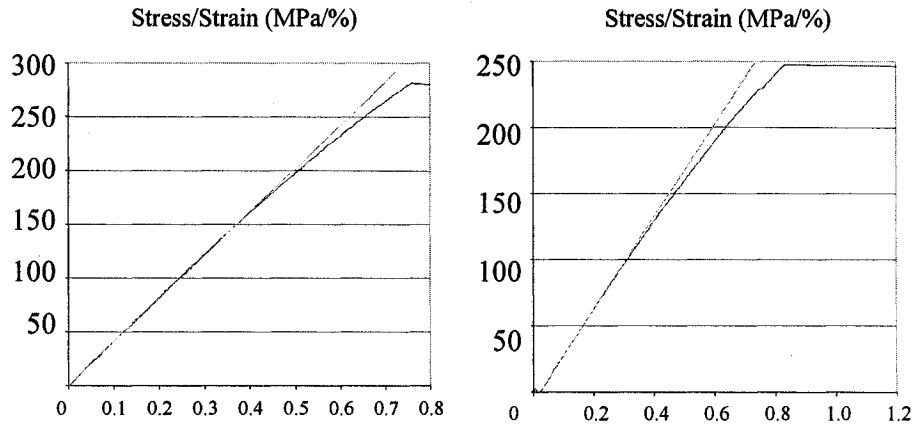
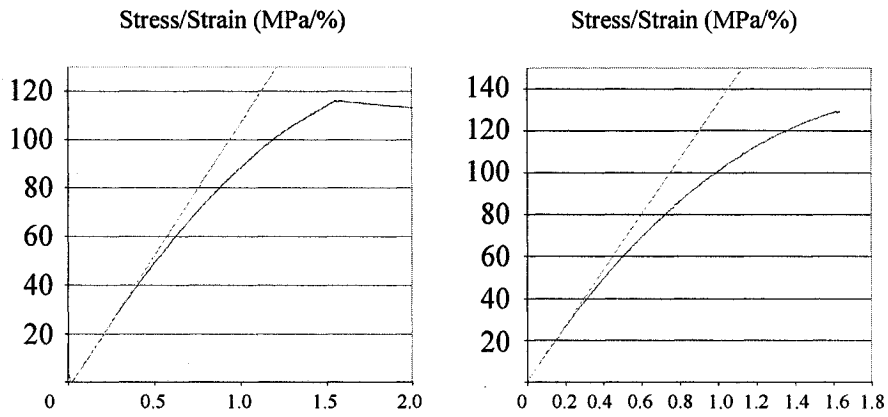


Figure 14: The standard test mold, picture frame and sample coupons

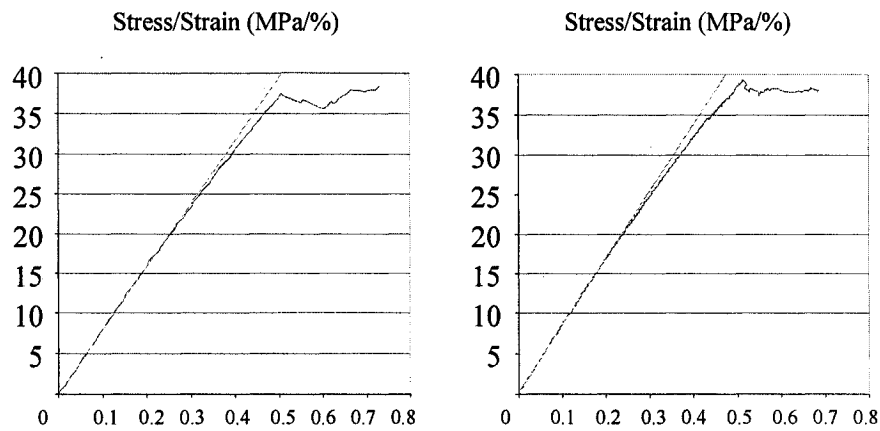
Plates were injected with different fiber angles such as 30, 45 and 60 degrees and coupons were cut from the plates. According to company information (see Table 2), 2 mm thick laminates made of four plies should represent a 48 percent fiber / resin ratio when the fibers are oriented at 45 degrees. As this project aims for a 50% fiber content, this is judged acceptable. For the case of 30 and 60 degrees, the fiber content was slightly higher, reaching close to 53 percent. Because of the tight time schedule, only tensile properties were measured. The experimental test results are presented in Figure 15, Figure 16 and Figure 17.



**Figure 15: Stress-Strain curve and linear interpretation for braided fabric at 30°**



**Figure 16: Stress-Strain curve and linear interpretation for braided fabric at 45°**



**Figure 17: Stress-Strain curve and linear interpretation for braided fabric at 60°**

It is of interest to notice how the samples (especially the 45-degree sample) do not behave in a linear manner. This concept is well referenced in the literature and is due to the non-linear elastic behavior of the sheared matrix [53,54]. The linear correlation was therefore estimated as well as possible, as shown on all three figures, in order to obtain the initial modulus. From the acquired data, composite laminate theory was applied to estimate the other properties. In order to do so, many assumptions had to be made and certain properties were found by interpolating from known properties of other fiber reinforced materials. A large spreadsheet allowed interpolating the data for other fiber angles, in increments of five degrees.

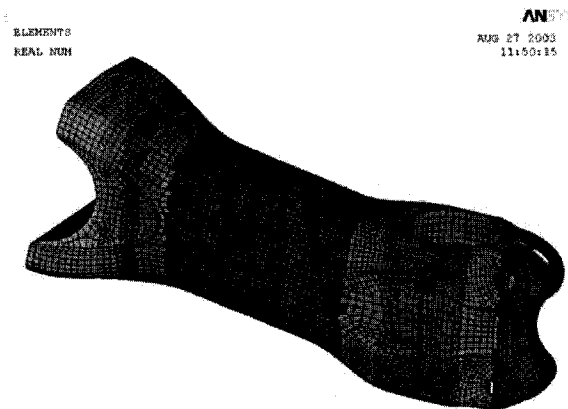
### **3.2 Model Development**

Two different finite element software packages were used to produce results. IDEAS was first used while the initial design was developed to determine the required lay-up. The model was a simplified one and the material properties used were assumed to be those of T300/Epoxy (the actual properties had not been measured yet). Using such an assumption was not a big problem considering that it was only used to validate the shape and identify general stress concentrations.

The second model was a more refined one because it came later in the design process. The exact shape of the stem was used to create the meshing in ANSYS. For several reasons, the loading cases were found difficult to model. First, it is important to model the clamping loads applied on the stem. The part is pre-loaded by the fasteners at its two ends, which already induces stresses even before it is put in service. Also, it was difficult to implement the inserts in the model. The resin joints are known to be very difficult to model, especially since their thickness is much smaller than the rest of the other elements [39,55]. To simplify the analysis, perfect bonding between the



elements was assumed. Another complication came from the modeling of the change in braid diameter. As a rule of thumb, it is known that a variation of 10 degrees in the fiber angle can result in a change in some properties of up to 20%. Therefore, it is an important factor that needs to be included in the analysis. To do so, the stem was separated in 6 different sections and different ply orientations (and properties) were assigned to each of them. In order to have an accurate model, the sections were chosen such that the braid angles would be accurate to  $\pm 5^\circ$ . The model is presented in Figure 18.

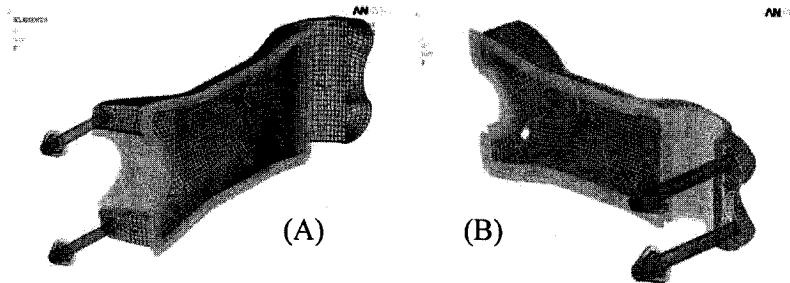


**Figure 18: The FEA model highlighting the different material sections**

Finally, another difficulty encountered was that there is no reliable available data on the extreme load cases on a bicycle stem. Therefore, it was difficult to simulate the behavior of the stem for case of an accident.

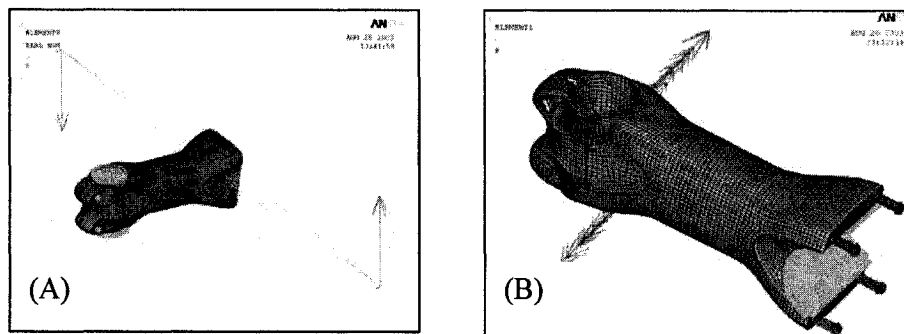
The problem was approached using three different load cases. First, the handlebar elements were fixed and given radial constraints. A load of 1400 N was applied at every fastener locations to simulate the clamping effect on the stem. Figure 19–A presents the loading case graphically. The same analysis was also performed on the external cap to look for induced stress concentrations. The second case consisted of applying the fastener loads to the steerer clamp. 2000 N loads were applied to each of the two

fastener locations, as shown in Figure 19-B. Note that in both cases, symmetry was used in order to reduce computing time.



**Figure 19: The clamping loads simulation cases**

Three service loading cases were: pure torsion, bending and actual riding loads defined by Van Der Aa [56]. The model for these cases is quite simple. The steerer tube is fixed and loads are applied using rigid elements (Figure 20). For the pure torsion and bending cases, arbitrary loads were applied and a linear relation allowed an estimate of the maximum loading. Riding loads are described as an out-of-phase loading of  $+164 \text{ N}$  /  $-147 \text{ N}$  in the vertical direction applied at the end locations of the handlebar. The rider is also assumed to pull towards himself with  $9 \text{ N}$  at each hand location. A standard  $44 \text{ cm}$  handlebar span was used in the simulation. This simulation is the most important one and shows the different stress concentrations in the part.



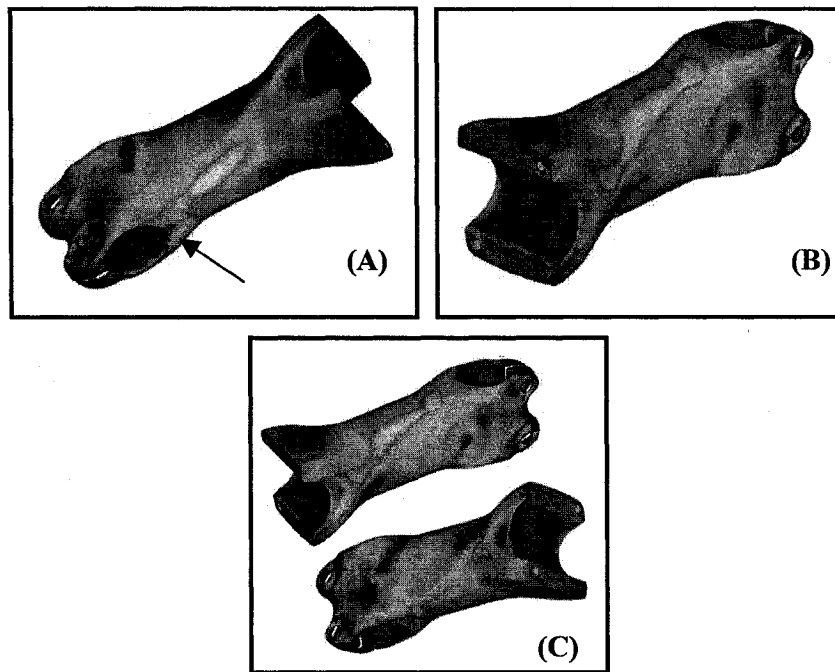
**Figure 20: The models for riding loads and full stem analysis**

Finally, the displacements from the steerer clamping loads and the reactions of the riding loads on the steerer tube are integrated in the clamped handlebar case as boundary conditions (Figure 20-B). This is an attempt to analyze the effects of the different loading cases all at once.

### **3.3 FEA Results**

Using the results from the first model (IDEAS), it was decided to adopt the 2" (50.8 mm) diameter braid for all four carbon fiber plies. Using this material allows for a 45-degree fiber angle in the "neck" (connection between the steerer tube and the boom section) of the stem. It seemed to be proper since this section was identified as an important region of stress concentration, especially in torsion. However, it is important to mention that this lay-up was only used in the early prototypes. As depicted in the section on testing (chapter 8), new prototypes were produced replacing two plies with two 2.5" (63.5 mm) braids. The reasons of such changes will be discussed later in this document.

The second set of load cases (ANSYS) was processed and displacements were obtained. However, most of the results seemed unrealistic in terms of displacements, probably due to the challenging material characterization. Nevertheless, the results of each case were used to draw conclusions about stress concentrations and location of ply failure. The Tsai-Wu failure criterion was used in order to determine ply failure and the results were found to be of great interest. The results of the service load cases (torsion, bending and riding loads) were particularly helpful to validate the design. Three graphical ply-failure solutions are presented in Figure 21.



**Figure 21: The FEA results under service loading depicting failure index in ply #1**

(A) Bending (B) Riding (C) Torsion

Before the production of the first prototypes, the lay-up could have been improved if a more precise model had been developed. The high risk of ply failure under bending loads (arrow, Figure 21-A) was initially judged to be normal, considering the presence of a large discontinuity in the fibers. However, early testing of the prototypes (section 8) showed a major case of de-lamination as the loads were transmitted from the steerer tube to the body of the stem by a thin resin bond. Modeling of the bonded joint would have helped to determine more precisely the location of the de-lamination. However, the model helped the understanding of the failure case and led to the re-design of the reinforcement plies.

The numerical analysis of the load cases allowed to separately identify the dangerous zones of the design and allowed for validation of the prototype shape. It was observed how material characterization was important in order to obtain reliable displacement and failure information and that a thorough set of material tests should be performed before attempting to build a FEA model.

## **4. MOLD DESIGN**

Tooling design for RTM is somewhat critical since the quality of the parts and the ease of manufacturing relies mainly on the quality of the tooling [21,30,31]. All aspects of the molding process should be planned before starting any practical work. Mold orientation (on which face will the pre-form be placed), heating and clamping method are only few of the important variables [57]. The mold must also have judiciously located injection and vent ports. The lack of existing design rules for location of these ports calls for an approach based on experience and trial and error [58]. However, computer simulation packages have recently been developed to help designers in this regard.

As mentioned in section 2.3, the stem is made using different inserts. Most of these inserts require their own set of tools and post-machining fixtures. The complete manufacturing process consists of five molds, three of which are made for resin transfer molding. Molds should be airtight so that application of vacuum in the mold does not pull any air inside the cavity. This is why the vents and injection ports were all placed on top of the mold, and not on the part line. By placing the ports in this way, it is possible to seal the cavity with a single silicone or viton o-ring. Viton is usually cheaper but tends to bond with the epoxy, making the de-molding process more difficult. However silicone is more fragile and extra care should be taken during the manipulation. A set of toggle clamps was used to close the mold quickly. This design did not perform as well as expected since it was not always possible to apply as much pressure as bolts would. Actually, they were found to make the manipulation and closing of the molds more time-consuming. All injection molds were also equipped with a set of two alignment pins, important devices essential to the precise mating of the two mold halves. The injection ports were made of brass with nylon quick connectors. By drilling the base of the fitting, it was possible to insert the tube all the way down to the part surface

while sealing and locking it at the same time. This was done so that the part would de-mold more easily, with less resin remaining in the fitting.

The desired fiber-volume ratio of the parts was 50%. The braid supplier specifies that the layer thickness at such a fiber ratio should be of 0.46 mm (Table 2). However, as discussed previously, the material thickness changes significantly when the braid diameter is modified. This is an important factor that should be taken into consideration, especially when setting the dimensions of the molded inserts.

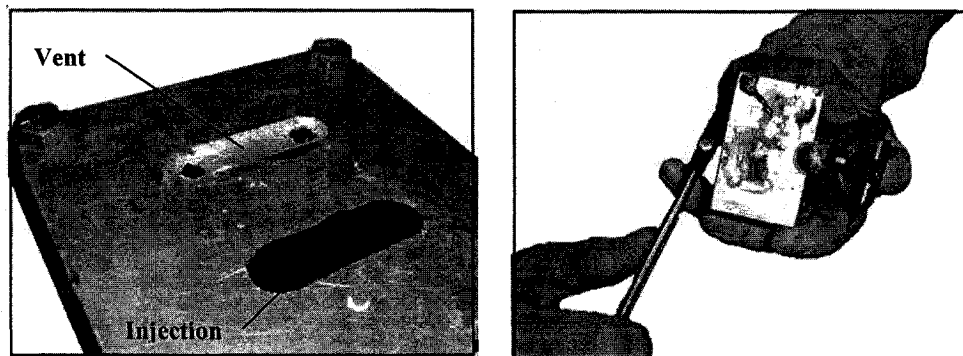
#### **4.1 Molded Inserts**

Two inserts are used as cores to compact the fibers against the mold cavity in certain locations (Figure 12). In the stem mold, it fills the area where the bladder cannot reach while for the external cap; it is used to give thickness to the part without compromising its weight. In order to obtain the right shape, the CAD model was used to offset the surfaces of the original parts. For prototyping purposes, only one insert was molded at a time. The material used is thermosetting polyurethane (Ren 6430, by RenShape solutions). This material is often used to make prototype molds by dipping. It shows good mechanical properties, especially in compression, and has a low density of about 1 g/cm<sup>3</sup> [59]. A few prototype parts also allowed observing a good chemical compatibility with the epoxy, leading to strong bonding with the composite layer. The material is originally white but can be colored black upon mixing in order to camouflage it in the carbon fiber design. This is done using ivory black paint pigments. An interesting observation was how the viscosity of the polyurethane decreased with the addition of the pigment. This is rather counter-intuitive but this effect of pigmentation on thermoset resins has been reported by other researchers [60]. The downside to this material is that it takes 24 hours to cure at room temperature. However, heating the mold

will accelerate the cure but the effects of this cure on the properties of the material have not been studied.

One of the difficulties in designing this kind of mold is to avoid air entrapment, which would result in an incomplete part. Since the liquid material is only poured, one cannot benefit from the advantages of pressurized plastic injection such as high production cycles and minimal air trapping. Also, the injection ports have to be strategically placed in order to be easily de-moldable and leave the shape intact when retrieved.

As showed in Figure 22-A the internal cap core is designed to be poured from one end and flow to the other. Small “pools” are used to connect the different injection ports and vents.



**Figure 22: The polyurethane inserts molds.**

- [A] Injection port and vent of the external cap mold  
[B] The ejector screw allows to retrieve the steerer insert

The steerer insert mold uses an ejector screw to be able to retrieve the part. A standard tap/screw arrangement is sufficient since no pressure is applied to the mold. This design proved to be very successful and should always be considered when designing molded-to-shape cores in aluminum tooling (Figure 22-B).

## 4.2 The External Cap

As shown in Figure 10 and Figure 12, the external cap is the part that is screwed over the handlebar to fix it in place. This mold had an important design constraint related to the aesthetics of the final part. The end of the top and bottom fiber layers had to join on the face mating with the stem body and not to the side so that the layer interfaces would not be visible in the final configuration. To do so, the mold cavity was designed lower than the part line in order to leave extra material in the bolt axes direction. A trimming operation could then be performed leaving the trim line invisible once the stem is mounted.

Figure 23 shows where the trim has to be performed in order to keep the part line invisible. The tool is made so that flat carbon fiber braided tape can be used to sandwich the polyurethane core. Braided tape was selected in order to match the appearance of the rest of the body and because of its extremely good draping properties. Good drapability is required to be able to conform to the complicated shape of the mold with no problems.

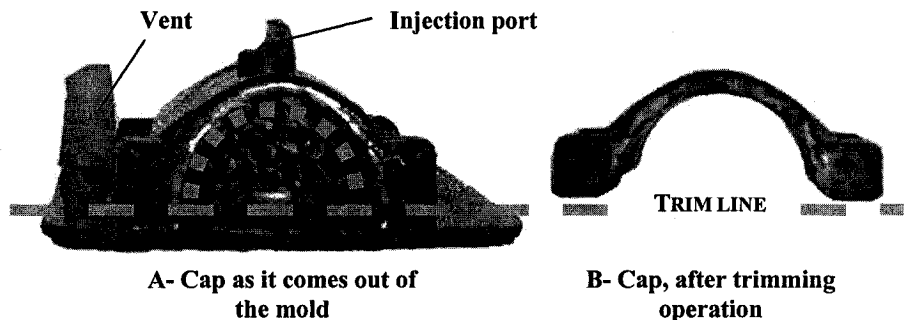


Figure 23: The external cap trim line

Consequently, the injection port and vent could not be traditionally placed from left to right. The injection port was placed in the middle of the part while the vent was placed at a surrounding cavity location (Figure 24). Only one vent port was initially judged to be sufficient.



No special means of de-molding is required to eject the finished part. Since the injection port is placed at the bottom of the female cavity, it can be used to push the part out manually.

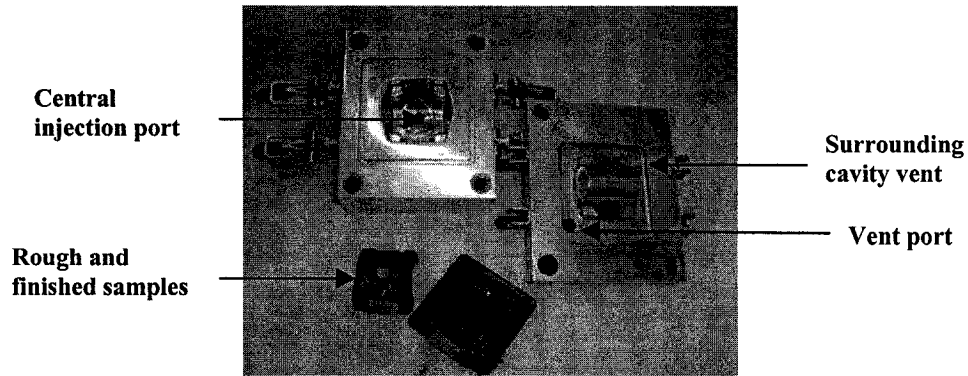


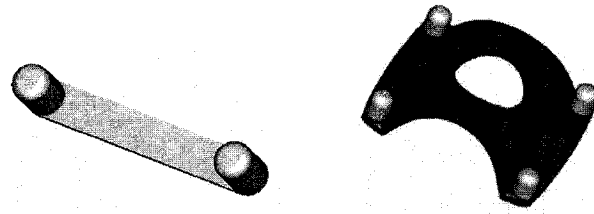
Figure 24: The external cap tool

### 4.3 The Internal Cap

The internal cap acts as an insert to the stem mold. It creates the surface that mates with the handlebar. It contains the four aluminum barrels (later to be threaded) used to attach the external cap to the stem. Combining composites along with metals has been a field of interest for years. When doing so, there are several factors the designer should not overlook. Void generation, galvanic corrosion, bonding compatibility and bonding surface area are some problems that should be monitored. Galvanic corrosion occurs when aluminum is placed in direct contact with carbon fibers. The electric compatibility between the two materials leads to corrosion at the fiber-matrix interface, weakening the ability of the composite to transfer load [61]. When studied in a laboratory, the specimens are soaked in salt water to speed up the effects. Under atmospheric conditions these effects can take several years to happen, however they still have to be taken into considerations. Meanwhile, Golubovic studied the bonding of composite with metallic inserts and showed that interesting mechanical properties could be achieved if the

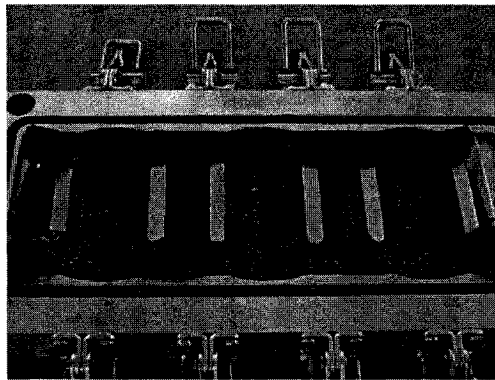
geometry of the insert was designed correctly [62]. Ferret et al. [63] studied the integration of metallic inserts in RTM and explained how manufacturing process can be optimized to reduce problems in vicinity of the inserts. Judicious positioning of the inserts combined to a careful fiber placement that avoids extra fiber compression are keys to the process success. In addition, several successful designs show that fiber/metal integration is possible. Oceau [64] showed that a titanium steerer tube could be effectively molded together with the composite legs of a bicycle fork. The theory of composite/metallic interfaces is also widely used in the aerospace field since connections between mechanical parts and composite components are often unavoidable.

Since it is a popular practice, many standard metallic inserts are available for composite material use [65,66]. However, the discussed prototype had several geometric limitations. The fasteners being small and placed in the four corners of the handlebar clamping face, no standard inserts could be used. The custom design had to maximize the bonding surface and allow for a problem-free installation in the mold. It was decided to connect the metallic barrels in pairs. The linking plate would prevent the insert from delaminating or slipping while providing a large bonding area with the fabric material. Because of cost considerations, the insert was made of aluminum. However, titanium would have been the material of choice since it would reduce the risk of galvanic corrosion [67]. In a production design, the aluminum insert base could be sandwiched between two thin layers of fiberglass to shield the aluminum from the carbon fibers. This technique is common practice in composite design. Another solution is to use an acid etching solution to treat the aluminum surface before molding. Figure 25 shows the design of the aluminum insert. It went under the working name of "dogbone", due to its particular shape.



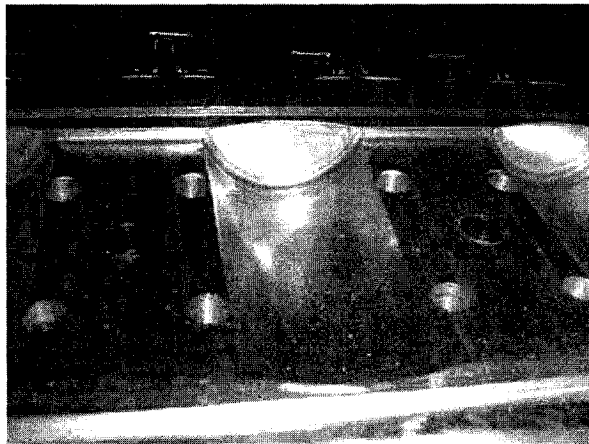
**Figure 25: The custom-made aluminum insert and the internal cap**

Figure 25 also shows the final internal cap design. The geometry of the mold to produce this part is quite simple. In order to reduce production time, three parts are made from one single injection. The inserts are slipped through the weaves of flat braided carbon tape and inserted into their alignment holes. This is shown in Figure 26.



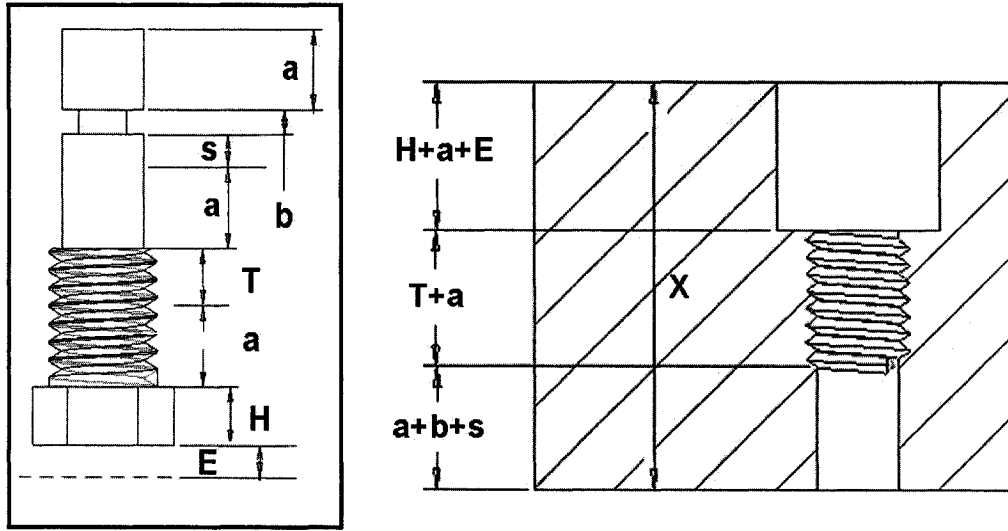
**Figure 26: The position of the custom inserts in the mold**

The connection between the two barrels also helps with the manipulation and positioning of the inserts. Resin pockets are found at the beginning and at the end of the cavity to ensure an even progression of the resin front through the fibers. Of the five carbon plies required to fill the mold, two are placed before the inserts. The mold also accounts for the change in thickness due to the inserts. This way, the permeability should not be affected and the resin should wet all the fibers evenly. A close-up of the finished mold is depicted in Figure 27.



**Figure 27: The internal cap mold and ejector devices**

The depth of the female cavity makes this part very difficult to eject from the mold, therefore, a set of ejector screws is required. Unlike the polyurethane inserts discussed previously (section 4.1), the mold of the internal cap is filled with pressurized resin. This means that the ejector screws must be sealed during the injection process. The design of such ejection devices can sometimes be tricky for the designer. Also, the ejector screws heads must be counter-bored into the mold so it can sit flat on the table during the lay-up and injection. To facilitate the approach, a short design method was devised. Figure 28 and Equation 2 describe the approach.



where

- a = Ejector travel**
- b = O-ring groove width**
- s = Distance of o-ring from the thread during injection**
- T = Thread engagement during injection**
- H = Head height**
- E = Extra counter-bore depth**
- X = Thickness to mold cavity**

Figure 28: The design of an ejector screw system

From the Figure 28, we can write

$$a = \frac{X - (b + s + T + H) - E}{3}$$

Equation 2: Maximizing the ejector screw travel

Using Equation 2, we can maximize the travel of the ejector screw(s) for any mold thickness. The designer arbitrarily defines all parameters except the ejector travel (a). This proved to be a very useful tool that would give exact dimensions. The ejector screws are machined using 1/2-inch (12.7 mm) cap or hex screws while the size of the non-threaded portion is set to 3/8 inch (9.53 mm). The o-ring placed around the ejector screw must remain

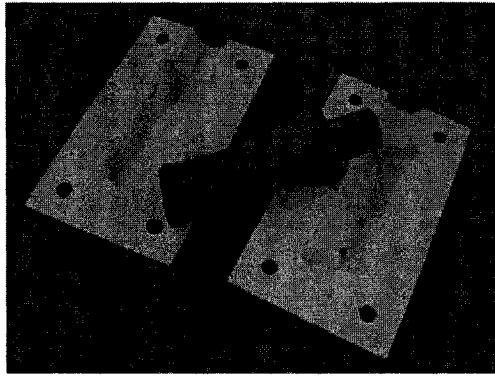
within the hole at all times to avoid degradation due to insertion. Application of some lubricant before installation also prevents premature wear of the seal. The depth and width of the o-ring cavity is made according to standard piston-bore assembly. Such design tools are available in any mechanical engineering handbook.

#### **4.4 Stem Body Mold and Bladder Holder**

The most important and innovative mold is the one used to make the stem body. The manufacturing process was optimized to enhance reproducibility and eventual integration into a production environment. The advancement in molding technology was motivated by the use of a flexible bladder to create the hollow region in the stem body.

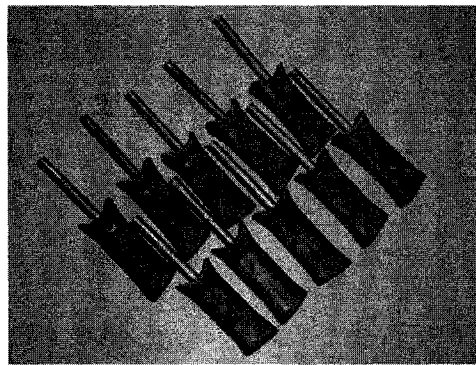
##### *Latex bladder as inflatable core*

To reproduce a negative of the stem's inside cavity, the surfaces of the CAD model were offset by 4 millimeters. From this reduced computer model, a mold was made using *Ren-Shape*, an easily machined compound that is commonly used to make low-cost prototype parts. The mold is shown in Figure 29 along with one of the rough parts. Rapid prototyping was also considered but the cost was found to be prohibitive. Moreover, such degree of precision was not required.



**Figure 29: The mold used to make the bladder dipping mandrels.**

A dense thermoset polyurethane called *ProCast Blue* (by RenShape) was used to make 10 mandrels. Since the part has two opposite curvatures, the molded part requires some machining afterwards. Different grinding, drilling and sanding operations were performed. A threaded aluminum rod was inserted at the end of every specimen. These mandrels, shown in Figure 30, were then used to manufacture the bladders.



**Figure 30: The ten finished bladder-dipping mandrels.**

The bladders are manufactured by dipping the mandrels in a liquid latex solution. Since it is a very specialized process, we sent the mandrels to Latex Technology, in California [68]. Latex has great properties when it comes to bladders. First, it is a fairly cheap material, especially if it is compared to silicone. It also has no chemical reactivity with epoxy resin and

its maximum elongation before rupture is of the order of 300 to 400%. This means that it can be easily adapted to the complex shape and corners of our design without rupturing. The bladders were made with approximately one millimeter-thickness, to make sure that they would be resistant enough to be reusable. It was also specified to the manufacturer that the metal rods had to be dipped as well and that the resulting necks should be about 30 mm long.

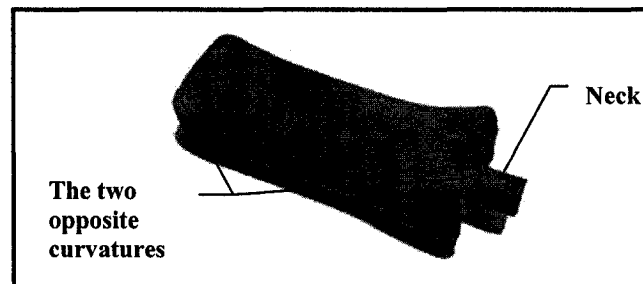


Figure 31: A latex bladder sample

### The fiber pre-form

Although some previous work on combined RTM-bladder processes suggest the use of a partially inflated bladder to make the pre-form [48], a slightly different approach was used here. The four layers of fabric are placed on a plastic mandrel, made from a reduced negative of the mold cavity (Figure 32-A). A thin layer of tackifier is sprayed between each ply to maintain the shape and fiber orientation (Figure 32-B). The level of tackifier should be kept to a minimum since it may act as a contaminant and can greatly affect the mechanical properties of the part [35]. Note that the two outer layers are one centimeter longer than the two inner ones to accommodate the fold-over described in the design section. The mandrel is then split and retrieved resulting in a usable pre-form (Figure 32-C).



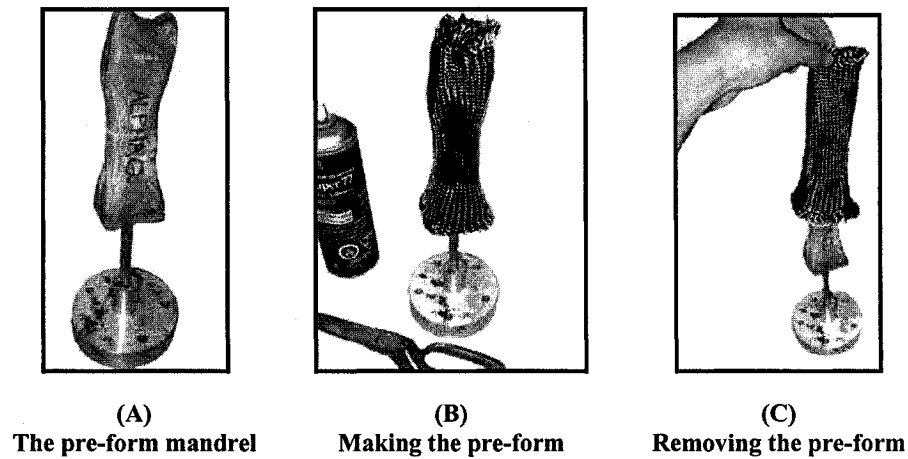
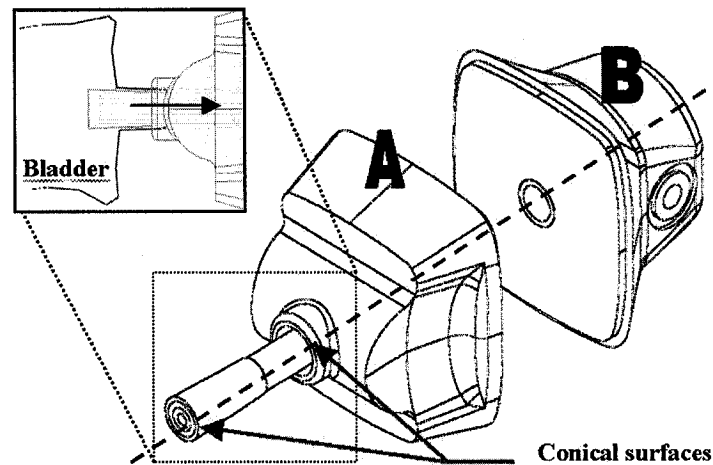


Figure 32: The pre-forming process

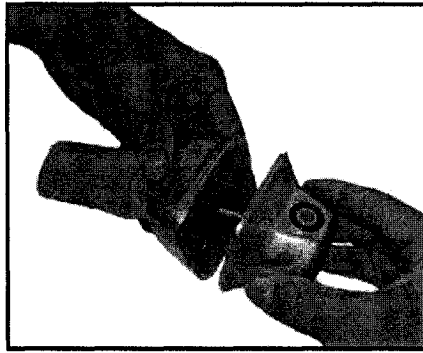
### The bladder holder

The innovation of the stem mold lies in the bladder holder. This part of the tooling has several functions. First, it holds the latex membrane in place by squeezing its intake knob between two conical surfaces (Figure 33). This ensures a leak-free joint that is practically foolproof in a production environment. Michaeli et al. explored this type of design in 1993 [48]. In a later paper, they even automated the sealing process by using a pneumatic piston arrangement [32]. Although Michaeli's design and the one presented here are similar in clamping method and application they differ in the way they are integrated to the mold assembly. In the present design, the tooling is placed entirely inside the mold cavity, while Michaeli uses an external fixture. The conical rod going through part A of the bladder holder (Figure 33) is threaded to fit into the second part (B) and acts as a mechanical connection between the two. By putting the two parts together, the cone is pulled in and this applied tension keeps the assembly altogether. Figure 34 depicts this novel connection technique.



**Figure 33: Exploded schematic of the bladder holder system**

The conical rod is also drilled through to inflate to the bladder. In fact, part B (Figure 33) also acts as a connection between the air compressor connected to the top of the mold to the inside of the bladder. The surface where the two halves of the bladder holder mate as well as the flat one where the air connector is located are sealed with o-rings to avoid any leaks during the injection. This is important since the bladder holder is within the sealed area of the mold cavity. Trek also uses a bladder connector that lies within the seal of the mold [3], but their rigidized bladder process is used with prepreg fabrics, rather than RTM. To the knowledge of the authors, the current method is the first time that such integration is used in conjunction with liquid composite molding. The design is rather complicated since resin flows everywhere within the sealed area. Therefore, the tooling must be demoldable and every connection must be sealed individually.



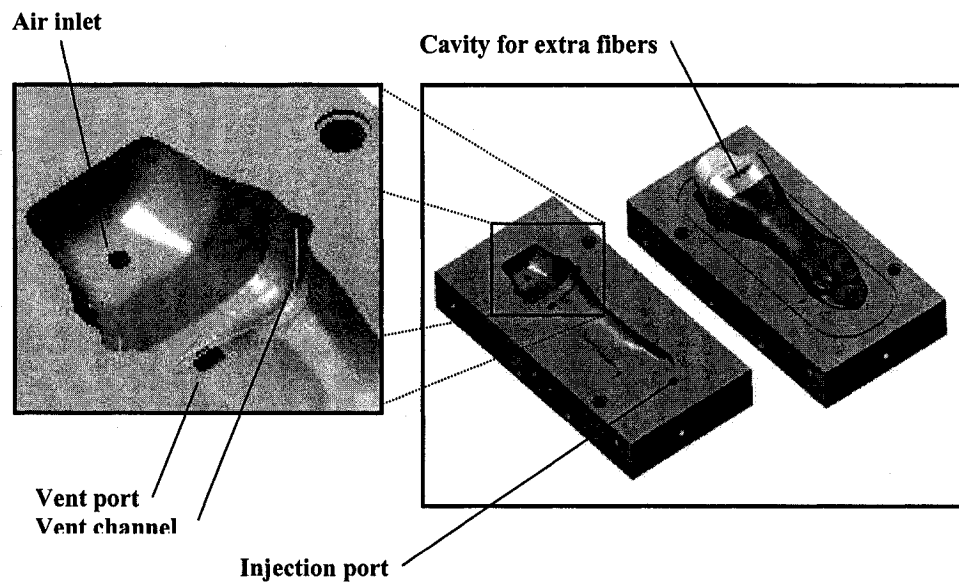
**Figure 34: Assembly of the bladder holder**

Finally, not only does it hold the bladder in place and serves as a connector for air supply, but the bladder holder also acts as a third face to the molding process. The front face is used to align and hold the internal cap. The latter is drilled in the middle to fit tightly around the circular extrusion coming out of the handlebar face. In this way, the external cap is centered and the metallic barrels are aligned in the mold. It is against this face that the fiber coming from the body is folded over the insert to assure undeniable structural integrity, as depicted by Figure 13-A. This last particularity, of molding a third face to the component at the same time as connecting the bladder makes the design even more unique and pushes the degree of part integration to a another level. Note that the seal around the two halves of the fixture is used to create a discontinuity in the resin flash to allow the operator to unscrew the assembly after the injection.

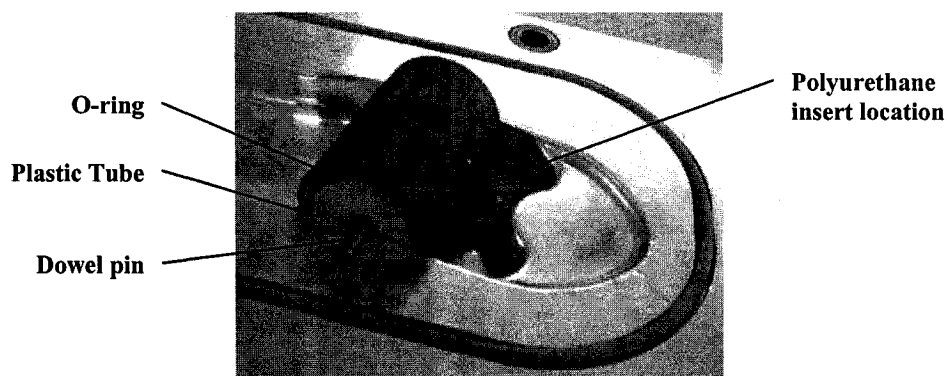
### *The stem mold*

The challenge of the stem mold was the positioning of the vents and injection port. To do so, hypotheses were made to predict the flow of resin. A parabolic protrusion was made at the steerer end of the stem. This channel was created to allow the flow of resin to advance evenly through the pre-form. On the other hand, the vent was somewhat problematic. In the stem lay-up

(seen in Figure 35), the extra fibers that are not included in the handlebar fold-over (Figure 13-A) are placed in cavities under and on top of the bladder holder. It was decided that those two regions would be used to locate the vent port. The bottom cavity was connected to the top by an empty channel (runner), imitating design was recommended by Michaeli for the production of carbon hollow tubes by resin transfer molding using an internal bladder [32].



**Figure 35: The stem molding and general geometry of the molds**



**Figure 36: The alignment system for the carbon steerer tube insert**

In order to position the carbon fiber tube adequately during the injection process a special plastic plug is inserted into the tube (Figure 36). Dowel pins are passed through the fiber pre-form and center the plug. Small grooves are machined in the stem mold to support the dowel pins and assure a perfect alignment of the tube. The plastic plug has two o-ring grooves located on top to prevent the resin from flowing between the carbon tube and the plug. The polyurethane insert is placed against the steerer tube, inside the pre-form. It self-aligns between the fabric plies.

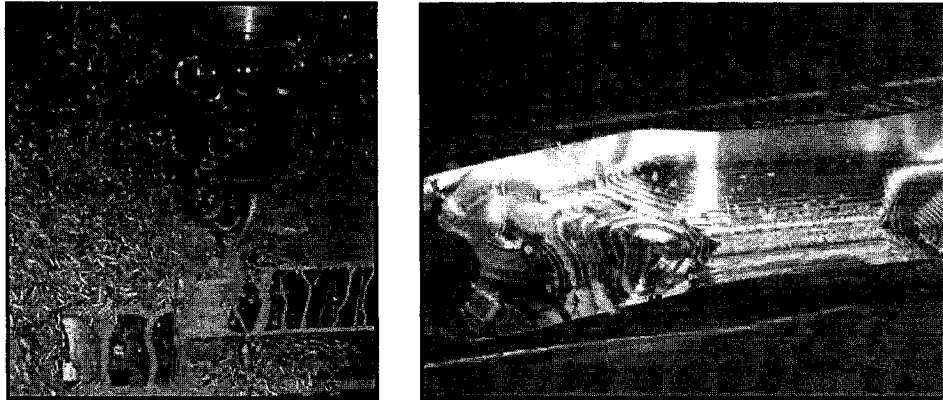
Apart from the above anomalies, the mold was designed in a similar fashion as the molds described in the previous sections. No ejecting mechanism was planned but it should be a requirement in a production environment. It is suggested that two screws should be placed under the injection port protrusion and under the flat surface of the bladder holder.

Also, it was found that a wider injection port would have been beneficial for reducing pinching of the fibers at the end of the pre-form.

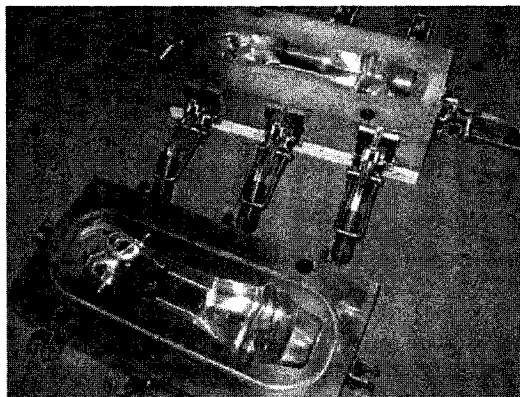
## **4.5 Mold Machining and Finishing**

As shown in Figure 37, the molds were machined using Computer numerical control (CNC) machines. The complex CAD files were exported to MasterCam, where the tool paths were optimized. Due to the complexity of the surfaces, most finishing tools were ball end-mills. Even with extreme caution, the tools leave many ridges called “scallops”. After the machining operations, the mold must be sanded. In order to obtain a great surface finish, different grit sizes are used in sequence. Insert molds were sanded up to 600 grit while visible parts of the stem (body and external cap) were brought to a mirror finish of 2000 grit. Apparently, a minimum 1000 grit is necessary to obtain a glossy surface finish on the final component [30]. Once the sanding

is complete, the mold surfaces can be polished and a stem can now be injected (Figure 38).



**Figure 37: External cap mold on the CNC and scallops left in the stem mold after machining**



**Figure 38: The finished stem body molds**

## 5. INJECTIONS

In the RTM process, resin is pressurized and forced through a fiber pre-form. Consequently, a resin injection machine is required. Many models are available on the market [69,70]. The one used for this research is the Radius 2100 [71], a long air piston equipped with a displacement indicator and a controlled heating jacket. Collecting information on temperature, displacement of the piston and pressure is important because as they represent the three main control parameters during the injection.

### 5.1 Resin Selection

The choice of a resin system is an important step of design with RTM. Many resin systems were investigated and parts were produced with several of them. The ideal resin for our application would have the following properties: low viscosity, short cure time at less than 100 °C, high modulus and high gloss. These are typical desirable requirements common to many RTM designs [72].

Viscosity is known to be a determinant factor in flow behavior through the dry fabric. Generally, viscosity is given in function of temperature, as those two properties are highly related. The lower the viscosity of the resin, the easier it should be to go through the pre-form. Typically, commercially available resins can have viscosity values as low as 10 mPa-s. Injecting under temperature also tends to temporarily decrease the viscosity of the resin before the cure is triggered. This change of phase is generally sudden and the time elapsed since the mixing is called the *gel time*. The cure dynamics also changes in function of the heat applied during the process and mechanical properties can therefore be affected. A short cure time is also an important requirement in order to accelerate the production. The limiting factors for cure temperature are the melting point of the injection tubes and cooling of the mold before the next injection. Teflon tubes have melting points

of over 260 °C but are very expensive. Since the tubes are consumables in the injection process, it is important to minimize their cost. Polypropylene tubes were found to be the material of choice, with a fairly high melting point of 100 °C and a price of about one fifth the price of Teflon [73]. It is also important to take the cooling time of the mold into consideration when setting the cure limits. A longer cooling time could mean that fewer injections can be performed successively. Furthermore, a resin with interesting mechanical properties was required since the part should minimize deflections under high loading. High modulus for a cured resin is generally judged to be around 3 GPa. In addition, since one of the secondary goals is to produce parts that require as little surface finishing as possible, a high gloss resin would be appreciated. This way, it is possible to take full advantage of the process.

The selection process was also based on the cost of the resin and availability at the time of production. There are also several other important parameters that have to be taken into account such as fiber wetting, pot life and ease of machining of the resin, but they are more specific to each resin systems. The considered resin systems are shown in the following table.

<i>Name</i>	<i>Company</i>	<i>Type</i>	<i>Typical use</i>
DERAKANE 8084	Dow	Modified Vinyl-Esther	Laminating
EPON Resin 862 / EPI-CURE Curing Agent W / Accelerator 537	Resolution	Epoxy	RTM / Filament winding
EPON resin 9504 / EPI-CURE Curing Agent 9554	Resolution	Epoxy	RTM / Infusion
TDT 177-114 (Miapoxy 100)	Vantico	Epoxy	Laminating

**Table 3: Resin systems evaluated**



It is important to note that several epoxy systems could be suitable for this process. However, it was judged that a comparison between four different compositions was acceptable, considering the scope of this project. The following table presents the different properties of the matrix materials considered.

	Flexural			Tensile		Viscosity mPa-s @ °C	Pot life hrs @ RT*	Gel Time min @ °C
	Cure hrs @ °C	Modulus GPa	Strength MPa	Modulus GPa	Strength MPa			
Derakane 8084 [74]	0.5 @ 90	3.3	132	2.9	76	360 @ 25	0.5	2 @ 90
Epon 862 [75]	8 @ 121	3.14	122	1.95	59	50 @ 80	7.9	30.5 @ 121
Epon 9504 [76]	5 @ 71	2.94	120	2.93	79	350 @ 25	1	30 @ 71
Miapoxy 100 [77]	24 @ 25	N/A	N/A	N/A	N/A	800 @ 25	0.5**	38 @ 25

\* RT = Room temperature

\*\* Estimated, from experience

**Table 4: Important resin properties**

All four matrices were used to make prototype parts. From inspection of the de-molded parts, it was possible to make a choice.

### Derakane 8084

The first prototypes were made using this modified vinyl-ester. An elastomer is used in this resin formulation to increase the strength and impact resistance. It was first thought to be a great resin since most ester-based resins are rapidly cured with heat and are usually cheaper than epoxies. However, cutting of a specimen made with this system showed that the

impregnation of the fibers was not through and that the part was not fully consolidated. On top of that, it was observed that the resin was chemically reacting with the bladder, leaving the inside of the stem tacky. This indicates contamination of the resin thus leading to poor mechanical properties. Although this matrix led to a glossy surface finish, large regions of resin shrinkage left some characteristic marks. Shrinkage is a characteristic of ester-based resins and can create high level of residual stresses [78,79]. It is possible to combine additives to reduce this effect but it was judged unnecessary because of the other problems with this resin.

### EPON 862

This resin was initially thought to be the most suitable for our application. It was designed especially for RTM, with a viscosity comparable to water at 121 °C. The problem is that a fast cure can only be attained with temperatures in the range of 175 °C. As stated before the low-cost tubing cannot sustain such temperatures. Still, a couple of samples were made using a 121 °C cure for eight hours. The results were disappointing as the part came out with a very poor surface finish. Therefore an alternate solution was sought.

### EPON 9504

Described as high fatigue strength by the manufacturer, this resin can be cured in approximately 5 hours at 71 °C. It also has low viscosity at room temperature (350 mPa-s), which is easier to process since it requires no pre-heating of the mold. The part quality was found to be satisfying but the main problem was in the de-molding process. When impacted, the solidified resin would shatter to a powder. This was found to greatly complicate the de-

molding and cleaning of the mold. Moreover, when machined, the resin would melt and leave residue on the tools. Diamond coated tools would therefore get clogged with resin. Considering the numerous machining operations to be performed on the parts and the complications encountered, this resin was not considered further.

### Miapoxy

This general use structural epoxy showed impressive behavior for the application. Having the highest viscosity of the four tested systems (a measured 739 mPa-s at room temperature), it was not expected to give good results. However, it has given fully consolidated parts with the glossiest surface finish. It was a concern that this resin is marketed as a 24-hour, room temperature cure and might not be applicable to a production environment. Still, the supplier confirmed that it was possible to use a higher temperature to accelerate the production process without affecting the mechanical properties.

## **5.2 Injection Parameters**

In order to have a repeatable process and good mechanical behavior of the parts, guidelines should be outlined concerning the process parameters. Injection pressure and temperature are the two controlled parameters. In all injections, they are meant to give a slow and thorough displacement of the flow front. The injection is stopped when there are no more bubbles coming out of the vent port. It is believed that clamping the vent tube for about a minute upon arrival of the front is beneficial since it allows the small bubbles to collapse together. This way, air is easier to drain afterwards. Once there are no (or very few) bubbles coming out of the vent, the tube can

be clamped permanently. Injection pressure is typically increased to reduce the size of possible small air bubbles and/or defects.

The temperature control profile was identical for all molds. To produce the prototypes, the cure was performed with a single heating plate, placed underneath the molds. To assure a good thermal contact, a heat sink compound was used. Also, insulation plates were made for every mold in order to reduce the amount of heat loss. A typical cure cycle for the selected resin will begin with room temperature (or slightly higher) injection. Immediately after clamping the vents, temperature is increased to 80 °C. Using the hot plate, it takes approximately 30 minutes to reach the set temperature isothermally. Using integrated heating elements can significantly reduce the heating time, therefore shortening the cure process. A hundred and twenty (120) minutes later, the molds are retrieved from the heating plate and cooled for 15 minutes. The part is ready to be de-molded but it is important to mention that a post-cure (although it was not performed) would be an important addition to the process. Post cures are usually meant to finish the consolidation of the part by completing the chemical linking inside the resin.

### *Internal cap*

This mold was very easy to inject. The fairly simple shape of the mold did not present any complications. The mold was injected at 240 Pa and the injection pressure was not varied during the advancement of the front. A 450 Pa static pressure (after clamping) was applied. It usually took less than two minutes for the front to go through and very little time (less than 1 minute) before the air is completely evacuated from the mold.

### External cap

A major issue encountered with this mold was the variation in the perform thickness. This variation created large changes in permeability and made it difficult to get a reproducible process. Therefore, it was decided to operate the injection at 410 Pa at the beginning and slowly climb up to full pressure (690 Pa) until the flow exits the vent.

### Stem body

Optimizing the injection parameters of this mold was one of the main goals of our research. As mentioned in the introduction, implementing bladder molding and RTM is not an easy task. It is found to be quite more challenging when the part is small. On top of the normal RTM parameter optimization, the pursued goal is the balance between the air pressure in the bladder core and the injection pressure from the pump [32]. Two methods are referenced in the literature.

One method consists of injecting the resin at a higher pressure than the bladder pressure [80]. This creates a fast resin flow outside of the fiber pre-form. The vent is then clamped and the bladder pressure is increased to wet the fibers completely. This method was tried and results were not acceptable. In fact, after cutting one of the prototypes made with this technique, it was discovered that the two internal layers were not fully impregnated. With a low bladder pressure, there is nothing preventing the resin from flowing preferentially around the fibers rather than through the fibers. Such a part loses all of its mechanical advantage, as the stresses cannot be transferred to the reinforcement. No further efforts were put into optimizing this technique since another approach was also possible.

In his extended work on the combination between bladder molding and RTM, Michaeli states that the pressure of the bladder should always be at

least 0.2 MPa higher than that of the injection pressure [46]. This way, the flow is forced to go through the pre-form and a complete wetting of the fibers is expected. This pressure should be kept as low as possible while still preforming complete fiber draping. The increase in bladder pressure tends to compact the fibers and decreases permeability of the preform, which results in larger energy requirements. His work also encourages increasing the bladder pressure after the injection is clamped to obtain a better (higher) fiber/resin ratio and superior consolidation of the part.

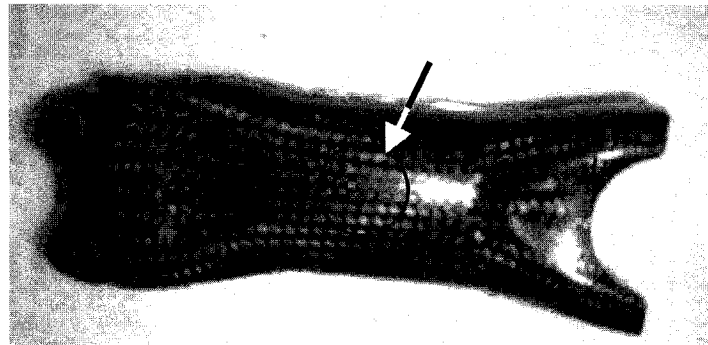
Considering the amount and quality of the information available, the latter technique was adopted. The optimal pressure parameters were found to initially set the pump at 205 Pa and the bladder at 410 Pa. Once the injection is clamped, the injection pressure is slightly increased to 275 Pa and the bladder pressure is adjusted as a function of the desired surface finish. It was observed that the surface finish and the weight are inter-related and strongly dependants on the difference between static pressures. Therefore, a nice glossy surface finish will require approximately 450 Pa of bladder pressure while a low resin/fiber ratio will require around 520 Pa. The choice of this parameter is mostly a function of the amount of surface finish one wants to put on the part. However, since all sports equipment has to go through a secondary paint job, it is preferable to use a higher static bladder pressure.

It was also noticed that this particular mold caused resistance to evacuate all the air from the pre-form. Bubbles would come out of the mold for a long time before settling, which would waste a lot of resin. After inspecting the possibilities of leaks from the bladder holder and its various connections, it was thought that it might have to do with the design itself. Other problems were also noticed on the manufactured parts. In fact, it was a priority to find the cause of the following recurring defects.

### 5.3 Recurring Defects

#### Dry patch in the stem body

A defect of great concern was a dry patch that would appear on the middle of the stem body (Figure 39). Two hypotheses were considered. It was possible that the resin was going ahead of the front by the flash and closing further along to trap air in the part. The flash region is defined as the space between the molds within the o-ring where the two molds mate. Typically, this region will fill with a thin resin film that is removed upon de-molding. However, this film sometimes came out thicker, especially due to fiber pinching between the mold halves.

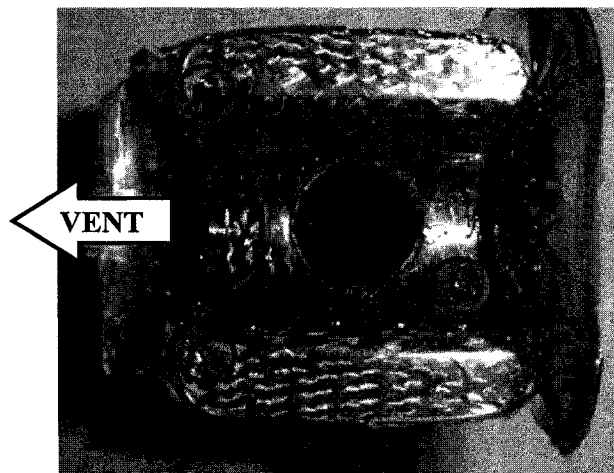


**Figure 39: Location of the recurring dry patch**

The other possibility was that the tackifier used in the pre-form making process (section 4.4) created regions of reduced permeability that blocked the resin flow. This effect is investigated, along with other effects of tackifier by Shih and Lee [34]. To determine the exact source of the problem, a flow simulation had to be run and is described in Chapter 6.

### *Voids in the handlebar clamp*

Several injection attempts of handlebar clamp exhibited voids, especially close to the vent (Figure 40). Those defects are hypothetically caused by the difficulty the flow to fully impregnate the bladder holder face. This will be studied in the next section (Chapter 6) about flow simulation. This theory is somewhat confirmed by the large amount of bubbles coming out of the vent before the injection can be clamped. Moreover, the surface mating with the handlebar also had a film of resin that was rather thick and uneven. The resin film is too thick because the hole in the internal cap does not fit exactly to the bottom of the alignment knob of the bladder holder. Rounding the edge of the hole inside the cap solved the problem.



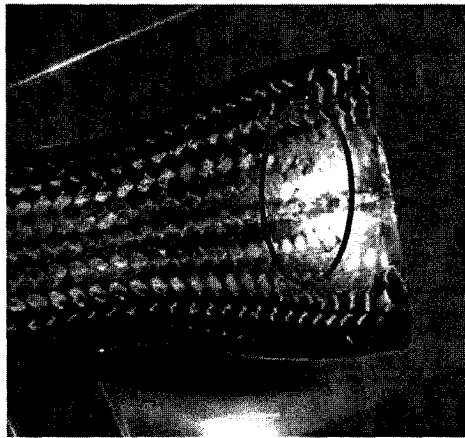
**Figure 40: Voids in the handlebar face of the stem**

Finally, it was observed that the edges were quite resin-rich. This is due to a lack of fibers coming from the body in the fold-over process. Use of tackifier in this region made the following experiments successful as it prevented slipping of the fibers during the lay-up process.



### *Voids on handlebar mouth*

The stem often exhibited voids on the top and bottom of the handlebar region. Figure 41 shows the problematic area. These voids were caused by the extreme change in angle of the braided fabric. The diameter of this region is quite large and in addition the fiber fold-over also tends to increase the fiber angle. Such a sudden change in angle causes disruption of the flow front and tends to create imperfections in the fiber impregnation.



**Figure 41: Problematic region on the handlebar mouth**

Similarly, Jinlian, Yi and Xueming showed numerically and analytically that the cross flow of resin and fibers in a woven laminate tends to cause voids [81]. Replacing the outermost and innermost layers with a larger diameter braid effectively solved the problem. Although the change in fiber angle was just as drastic in these layers, the more favorable permeability along the resin front direction improved the injection dynamics and filled the voids.

## 6. FLOW SIMULATION

Since RTM has gained in popularity, there has been a growing need to understand the behavior of the flow of resin through the pre-form. Since RTM is a closed mold process, it is difficult to visually comprehend the motion of the resin. Generally, a better understanding of the manufacturing process translates in a better control of the production. In composites, this means an automatic improvement in the mechanical properties of the resulting structure [82]. This is why numerical simulation tools were developed. Such simulation tools can help the designer to accomplish several tasks [36,83,84,85]:

- ***Position the injection points and vents in a way to avoid air entrapment and ensure a complete filling of the mold.*** S. G. Advani [86] showed that vents, especially those under vacuum, have a great influence on the flow displacement through the fabric material. This effect is even larger when it comes to pre-forms of lower permeability, such as in the present application. Poorly designed gates and vents can lead to areas of the part containing no matrix material.
- ***Obtain the pressure distribution during the injection in order to validate the numerical model.*** Knowledge about the pressure distribution can also be used to reduce the injection pressure, leading to an easier and cheaper manufacturing process. In a paper from M.K. Um et al. [87], it is proposed that a high inlet pressure can also cause wrinkles in the pre-form. Consequently, optimal process conditions are obtained by minimizing inlet pressure and favor a steady flow rate. Such parameters can be studied through flow simulation.
- ***Optimize filling time to enhance production cycles.*** This is more relevant for high volume applications or injection of large parts. By

simulating the flow displacement, it is possible to minimize the filling time and therefore increase the productivity.

- ***Debug mold problems and recurring defects.*** In the event that a mold is already in use, mold-filling simulation can be used to explain certain phenomenon and bring solutions to the designer. Although flow simulation is more efficient when it is used before the molds are manufactured, it can still be useful in post-design optimization. This is the most relevant reason why flow modeling is used in this research.

However, theoretical simulations have certain limitations when it comes to modeling practical applications. Deviations like non-uniformity in the fiber placement, race tracking over sharp corners or small geometric deviations can change the theoretically defined permeability values and give different flow patterns [53,88]. Such deviations from reality mean that the results should be treated as guidelines.

The theory to describe mould filling is based on flow through a porous media and is known as Darcy's law [36]. It states that the flow rate is proportional to the pressure gradient and inversely proportional to the viscosity of the fluid.

$$V = \frac{[K]}{\mu} \nabla P$$

where

[K] = permeability tensor (m<sup>2</sup>)  
μ = resin viscosity (Pa·s)  
P = Pressure (Pa)  
V = Flow front velocity (m/s)

Equation 3: Darcy's law

The permeability is a characteristic of the medium (pre-form) that usually needs to be measured experimentally, in a laboratory. It is always a function of the fiber alignment, fiber spacing and other complex geometrical

factors. The highest permeability of a fabric is along the fibers. Going across the fiber makes it harder for the fluid to flow, resulting in a lower permeability.

Most commercially available packages also take into account the thermal effect on resin viscosity. Such modeling will not be tackled in the present application due to the small size of the part and room temperature injection.

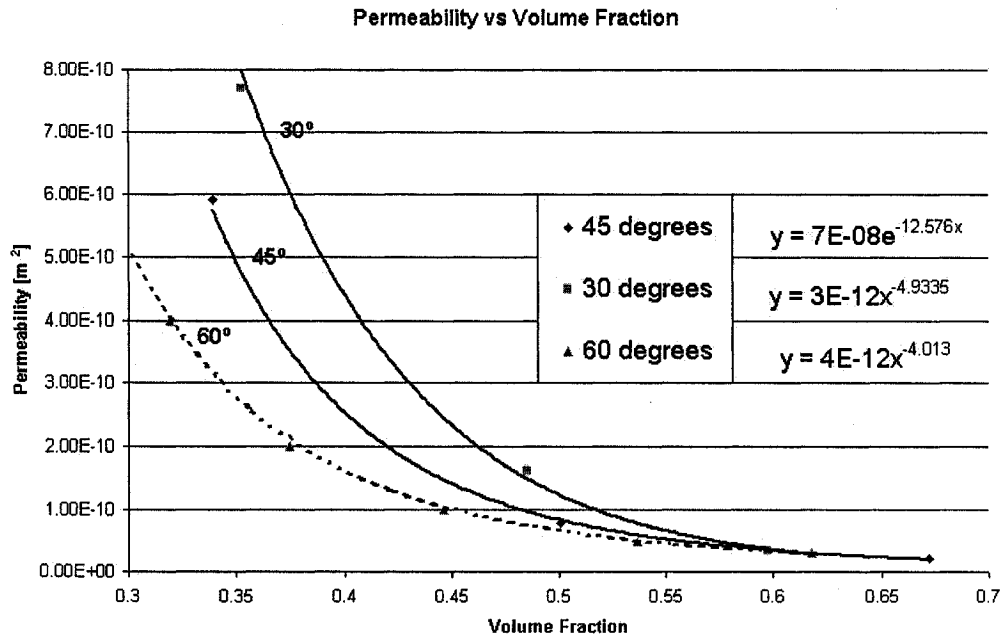
## **6.1 Permeability Measurements**

Since a flow simulation can only be as good as the permeability data it uses, it is important to run permeability tests on the materials [37]. Many theoretical models have been developed to estimate the permeability of the material. [53,89] One of the popular formulations is the Carman-Kozeny equation where permeability is only dependent on the type and geometry of the reinforcement [87]. However, a specialized experimental setup at Ecole Polytechnique was available and permeability tests were conducted there.

The experiment consists of varying the volume fraction ( $V_f$ ) of sample pre-forms at same fiber angle to get the permeability as a function of the volume fraction. Three tests are necessary to trace a permeability curve [90]. Preferably, samples volume fraction should be close to the one used in the process. The chosen approach was to keep the mold thickness constant and vary the number of layers placed in the cavity. A set of templates was used to cut all the samples with the same fiber angle. Injecting calibrated silicone oil in a transparent mold and monitoring the time taken for the resin to flow past predetermined distances provides the information needed for permeability calculations. The data processing is automatically done by the computed (data acquisition system) and results are generated instantly.

Tests were performed on both 45 and 30-degree samples. Two permeability curves were obtained by fitting power or exponential curves through the obtained results. The permeability values for other fiber angles

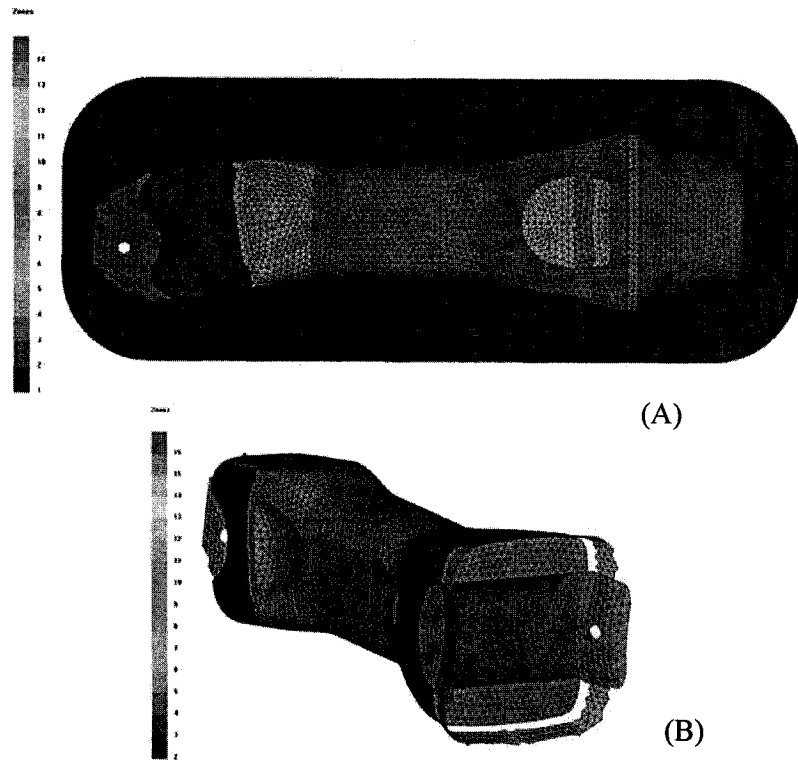
were extrapolated (such as at 60 degrees). The results are shown in Figure 42.



**Figure 42: Permeability of braided fabrics as a function of volume fraction**

## 6.2 Model Development

The PAM-RTM package was used to simulate the flow of the resin in the mold. A set of seven materials was used to model the flow behavior and predict recurring defects. From the initial mesh, different zones were defined. Each zone is associated with a material (Table 6) and is assigned a porosity value. The sections under the effect of bladder pressure are more compressed, thus are expected to be less permeable than the sections depending only on tolerances (such as where the plastic insert is placed). The next figure shows all the different zones defined on the stem.



**Figure 43: The two flow simulation models**

Zone ID	Name	Material	Porosity (Resin/Fiber Ratio)
1	Flash	Flash	1.00
2	Plastic Insert	Braid 50	0.57
3	Mouth	Braid 60	0.50
4	Handle Bar Face	Flash	1.00
5	Runner 1	Runner	0.98
6	Top Tube	Braid 50	0.60
7	Body	Braid 45	0.50
8	Bladder Holder	Flash	1.00
9	Fold Over	Braid 45	0.54
10	O-Ring	Impermeable	0.00
11	Side Vents	Braid 60	0.35
12	Lower Body	Braid 50	0.50
13	Runner 2	Runner	0.98
14	Diffuser	Braid 45	0.40
15	Dry Patch	Braid 45/Dry spot	0.50
16	Bladder Holder Knob	Impermeable	0.00

**Table 5: Properties of the different zones of the stem simulation**

The porosity is used to locally evaluate the permeability, using an interpolated function. The permeability data obtained during the material characterization was changed to be a function of porosity instead of fiber volume (porosity = 1 – fiber volume fraction). The fabric materials were defined using the relations obtained from the curve fitting process. Thus, for any configuration of the material, a permeability value can be generated.

Material Name	Permeability (m <sup>2</sup> )	
	[K1]	[K2]
Braid 60	8E-13 <sup>e9.1519x</sup>	1E-8x <sup>6.4928</sup>
Braid 45	7E-13 <sup>e10.088x</sup>	7E-13e <sup>10.088x</sup>
Braid 50	5E-13e <sup>10.107x</sup>	4E-13e <sup>11.239x</sup>
Flash	1.0 E-9	1.0 E-9
Impermeable	Defined as Tool Material	
Runner	2.0 E-6	2.0 E-6
Handlebar Face	1.0 E-10	1.0 E-10
Dry spot	1.0 E-13	1.0 E-13

**Table 6: Initial material properties**

The permeability of a runner can quickly be approximated by a Poiseuille flow in an empty channel [91]:

$$K = D^2 / 12$$

**Equation 4: Evaluation of empty channel permeability**

On the other hand, it is difficult to find an estimate for the permeability of the flash region. Therefore, the permeability was varied, trying to create a representative effect. The handlebar face permeability was judged to be small, since the two solid surfaces are pressed together by the bladder pressure. During the analysis process, the material properties were varied according to the different hypothesis. This way, solutions to several cases were computed and analyzed. The main results are presented below.

### 6.3 Simulation Results

The first goal was to see if a race-tracking flow (using the flash gap) possibly closed back on itself to trap some air. Using a flash permeability of approximately 10 times larger than the one through the fibers, it was seen that the flow was not likely to be responsible for the dry patch. This simulation did not take air entrapment into account. This kind of simulation is faster and helps to see the global flow of the resin in the mold. The results seem to be close to the actual progression of the flow front, steady and complete (Figure 44-A). A second simulation was performed, accounting for air entrapment while increasing the flash permeability by a factor of five. Although the permeability seems exaggerated, the results (Figure 44-B) show that it is rather unlikely that the small dry spot found in some specimens is due to the flash. Furthermore, dry patches would have occurred on both sides of the stem (as predicted by the simulation), which was not the case.

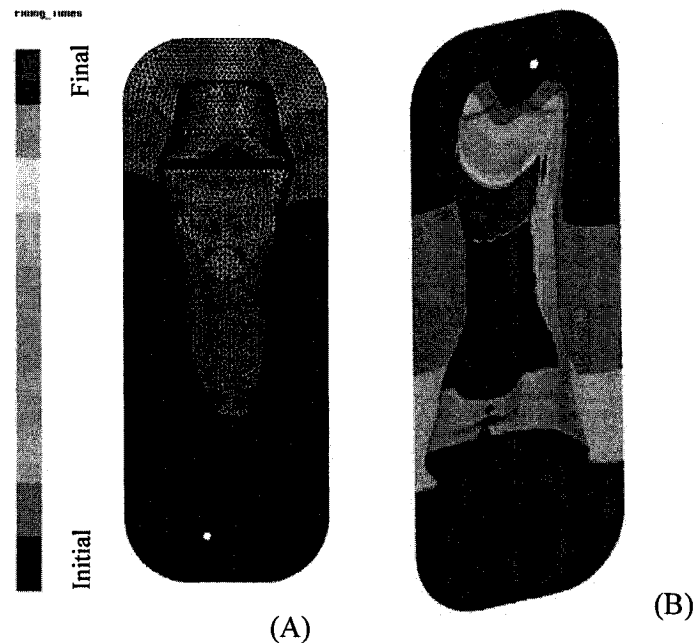


Figure 44: High permeability flash simulations



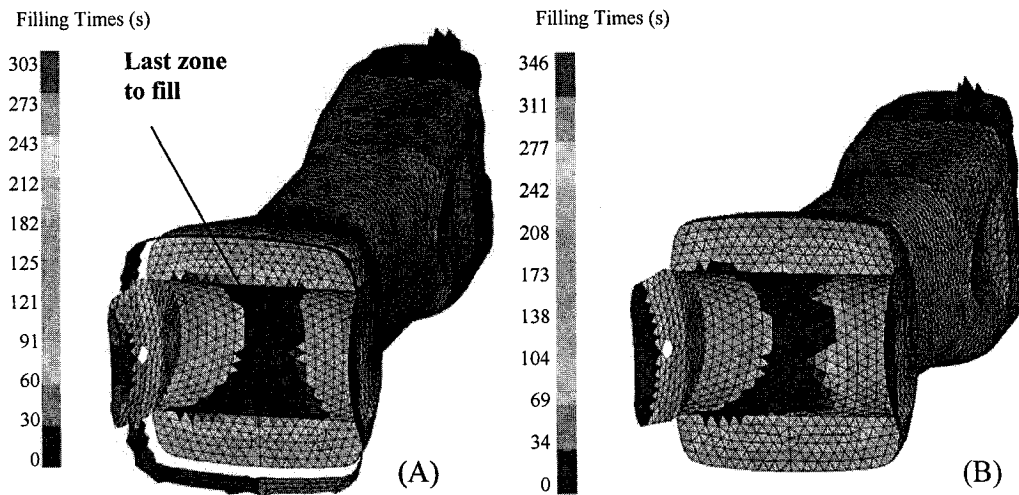
To validate the second hypothesis, a refined model with a section of higher permeability was inspected (Figure 43-B). The results matched almost exactly the location and size of the defect (Figure 45). A closer look at the process allowed to see that the method used to make the pre-form was inadequate as too much tackifier was used. Thus the permeability was affected. Tackifier was also only applied on one side of the body, which explains the asymmetry. Reducing the amount of tackifier used in the pre-forming process solved the problem.



**Figure 45: Filling of the mold with region of higher permeability**

The goal of the second simulation was to study the possible air entrapment in the handlebar clamp region. The model presented in Figure 46-A shows that there are some filling issues in the handlebar cavity. Although the air will eventually leave under higher pressure or vacuum, it remains a region at risk because of the way it fills. It was suggested that the flow would more easily go through the handlebar surface if it did not have a vent all around. The first (earlier) stem prototype mold had a comparable bladder holder design. Figure 46-B shows that blocking the circular runner can slightly improve the filling of the handlebar cavity. Although it is about to be implemented in the subsequent versions, one of the limits of the simulation code is the inability to handle the displacement of trapped air. Since the dry region is small (located almost completely between the faces of the bladder

holder and the internal cap), it is believed that vacuum application combined with resin flow rate will be able to eliminate it.

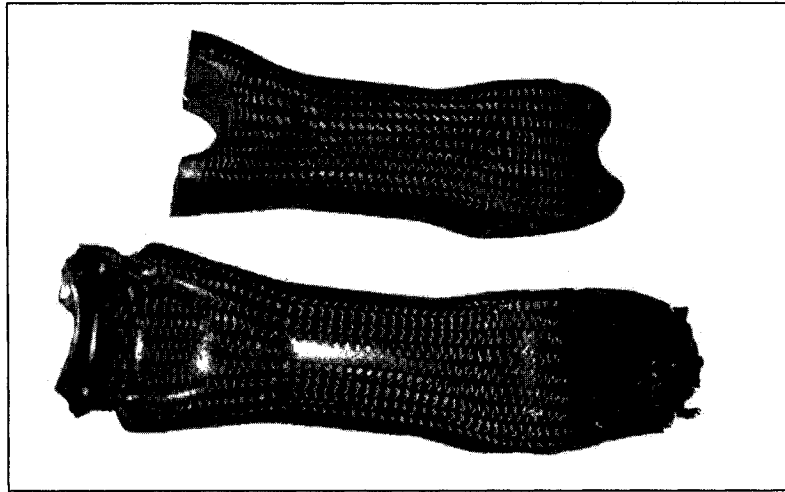


**Figure 46: Handlebar filling simulation showing possible air entrapment region**

The results of flow simulation provided some promising results and design guidelines. It also allowed to identify the source of various recurring defects identified in Section 5.3. However, in the future, it should be considered prior to building the tooling. This way, full advantage could be taken from the simulation, implementing the solutions directly in the mold design.

## 7. POST MACHINING FIXTURES

Upon de-molding, the stem has to undergo an extensive set of operations in order to bring it to its final shape. Figure 47 shows the rough and finished state of the stem, side by side.



**Figure 47: The rough and finished stems**

Similar finishing operations are performed for both the internal and external caps (Figure 23). In order to manufacture a number of prototypes and prepare the eventual production, a methodology had to be developed in order to achieve a fast, problem-free production cycle. A set of fixtures was designed to assure reproducibility in the process. In a production environment, those fixtures have to be designed for safety so that even an unspecialized worker can use them without risk.

This part of the manufacturing process is an integral part of the design and cannot be simply improvised. Post-machining steps have to be taken into account from the very beginning, before designing the tooling.

From previous experience, it is known that carbon fiber is very difficult to machine. The composite structure can be severely damaged if fibers are pulled out during the trimming or drilling processes or when the friction with the tool raises the local temperature drastically [92,93,94,95]. This is why very

high tool speeds are required. However, this also tends to create high tool wear. Consequently, carbide or diamond coated tools are preferred over conventional ones [96].

Due to similarities between the different fixtures, only the operations performed on the stem body are presented. This fixture shows a high level of integration. It combines all the operations that are typically used in the post machining process such as routing, drilling and sawing. Bear in mind that this design was made for the production of a few dozen of prototypes. In a production environment, most of the steps would be separated to accommodate a higher production rate. The post-machining fixture is shown in Figure 48.

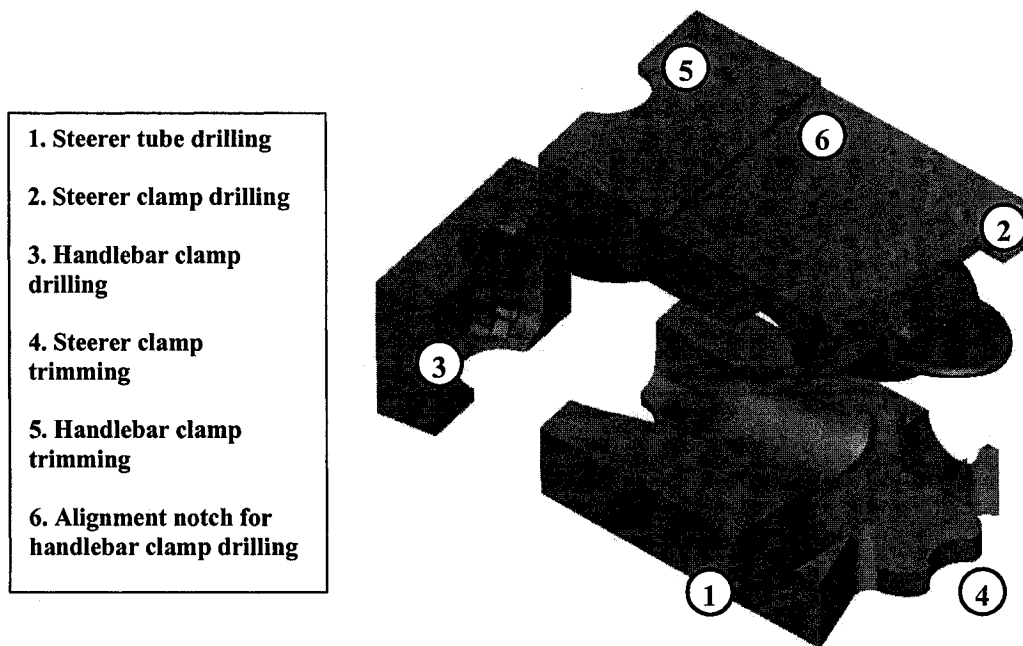
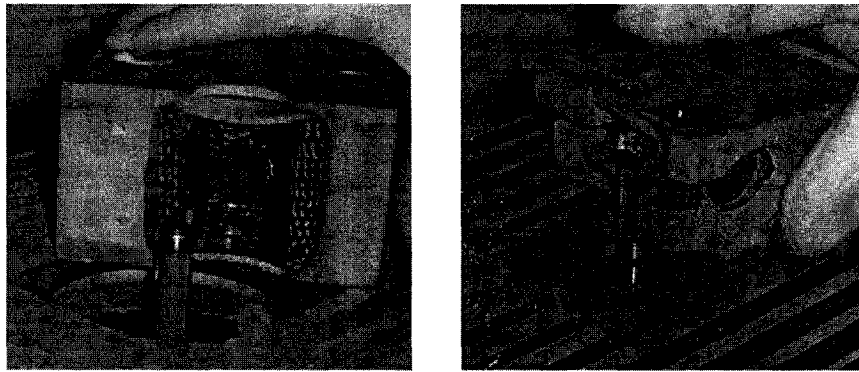


Figure 48: The stem post-machining fixture

The first operation after de-molding is to remove the alignment plug from the steerer tube. The fixture is used to hold the stem flat and level (Figure 48-1). A diamond coated hole saw is used to remove the four plies of carbon covering the plastic plug. The holes left by the alignment pins are used to guide the pilot drill. Once the centering plug is removed, the holes for

the steerer clamp can be drilled. An M6 carbide drill is used with the fixture providing exact location through the drill bushings (Figure 48-2). Removing the extra material left from the injection port completes the steerer section. In the description of the post machining operations on fork design, Octeau [64] suggested that the trimming operations be performed using NC machining. However, routing was adapted from the wood manufacturing industry and adapted to the composite manufacturing process. The tools are equipped with bearings and used by following template shapes (Figure 48-4/5). The extra fibers close to the vent port are also removed using this process. Figure 49 presents the operations being performed on the stem.



**Figure 49: Routing extra material on the stem using templates**

Using the groove (Figure 48-6) to align the stem vertically, the holes in the handlebar clamp can be made in the internal cap. The external cap is placed in the removable cap (Figure 48-3) and drilled at the same time ensuring perfect alignment of the holes. Removing the external cap, M4 taps are made using a tapping arm. The final operation is to cut the slot in the back of the steerer clamp. L-shape brackets are added to the fixture and the back of the stem is slid through a diamond coated tile saw.

Sanding the part line and any sharp edges finishes the parts. Minor surface defects can also be filled before the final clear coat is applied.

## **8. TESTING**

Good results from testing are important to assure repeatability and consistency in the properties of the parts. Once the first parts are made, it is important to verify if the design was valid by mechanically testing the part. In composite materials, this step is even more critical since the reliability of the part often depends on small design details and the manufacturing process. This chapter describes the techniques used for the testing of prototype handlebar stems and gives the results of the various tests.

### **8.1 Testing Methods**

Very few standard test procedures have been established for testing composite bicycle parts, especially stems. Consequently, companies such as Trek tend to develop their own standards and test fixtures that are more adapted to composite design and exceed the traditional specifications [97]. The testing procedure of the prototype stem was inspired from the ISO Cycles – Safety Requirements for Bicycles Standards [98]. However, making fixtures and test setups for all the suggested tests would have been quite tedious and very difficult considering the short time span of the project. This is why the procedure was based on the four ISO tests that were judged to be the most relevant.

- Static Pure Torsion
- Static Bending
- Torsion Fatigue
- Bending Fatigue

The test fixtures were made to accommodate an existing data acquisition system. The available equipment consists of a position feedback

pneumatic piston, a data acquisition card and a virtual instrumentation program (VI). The pneumatic piston has a 3000 N pushing capacity and a slightly lower pulling capacity.

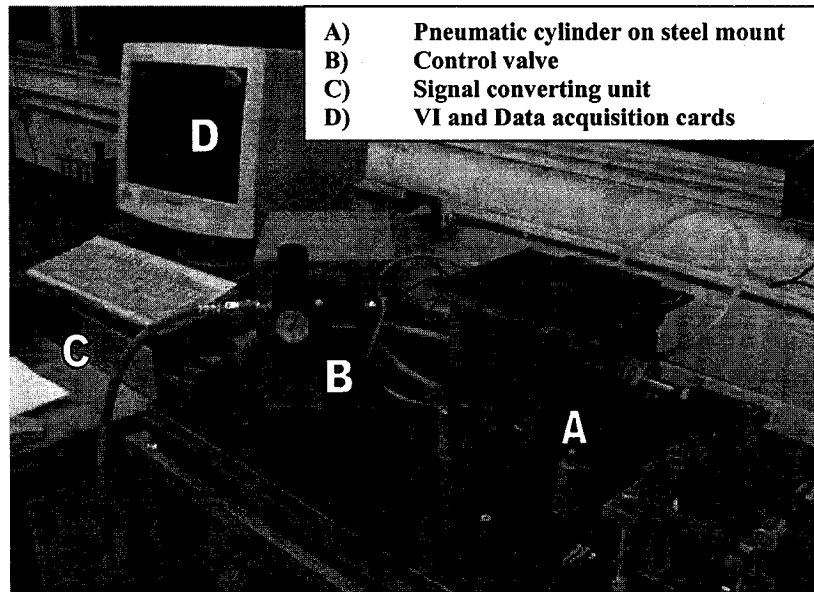


Figure 50: The test equipment

## 8.2 Test Apparatus

### Torsion

The goal of this fixture was to transform a single force application into two equal and opposite forces. This was achieved by building a combination of a lever arm and a pivot, as shown in Figure 51. The distance between each arms and the pivot is 3.5 inches while the distance between the piston arm and the pivot is 7 inches. The choice of 3.5 and 7 inches means that the stem is subjected to two opposite forces of the same magnitude as the one applied by the cylinder. From the piston load and displacement, the torque applied to the stem can be calculated as well as the angle of rotation of the stem at the point of torque application.

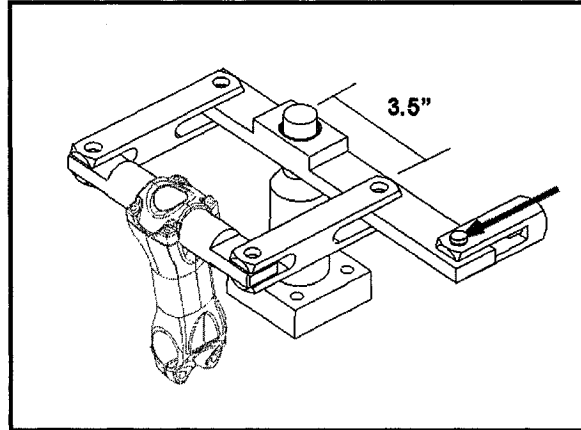


Figure 51: The torsion test fixture

The following simplified diagram (Figure 52) shows that torque and angle of rotation are essentially measured at the same location:

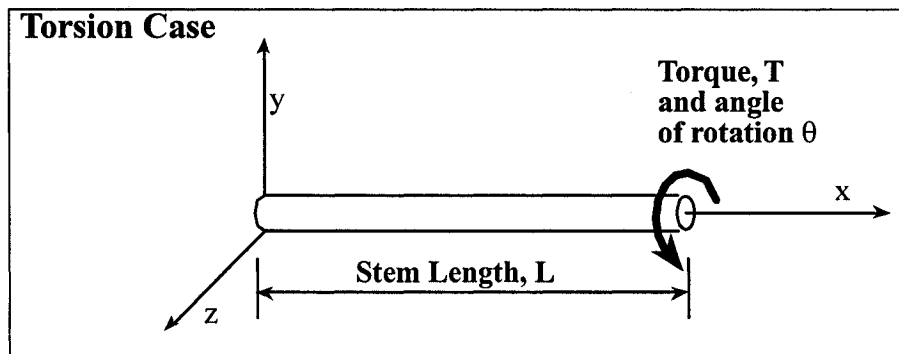


Figure 52: Simple case of clamped end torsion

From the values of torque and angle of rotation, the torsional stiffness (GJ) of the stem can be obtained from the following equation [99]:

$$GJ = \frac{T}{\theta} L$$

Equation 5: Torsional stiffness of clamped end torsion



where:  $GJ$  = Torsional stiffness

$T$  = Applied torque

$\theta$  = Angle of rotation

$L$  = Length of member

The torsional stiffness is a value that can be used to compare one test to the other or (in a possible future set of tests) to compare the current stem to competitor stems. Keep in mind that because the stem actually has a changing cross-section area, the value of  $GJ$  represents an “average” value over the length of the stem.

### Bending

The bending fixture is quite simple. It is a steel fork attached to a 1-1/4” cylinder where the stem clamps. It allows the piston to push and pull the stem for any desired load. The assembly can be seen in Figure 53. The load case is comparable to a cantilever bending situation (Figure 54).

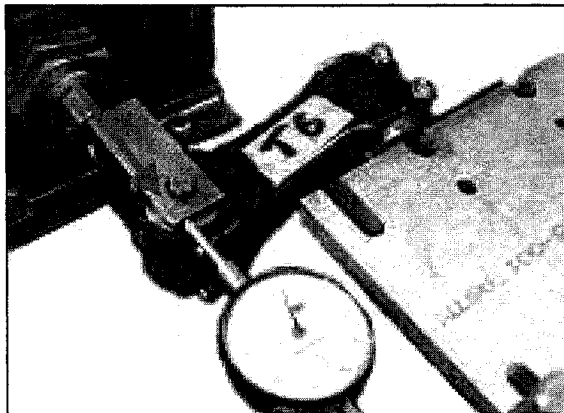


Figure 53: The bending test fixture

The displacement of the cylinder is the same as the displacement of the cantilever beam at the load application point. The following simplified

diagram shows that load and the deflection are essentially measured at the same location:

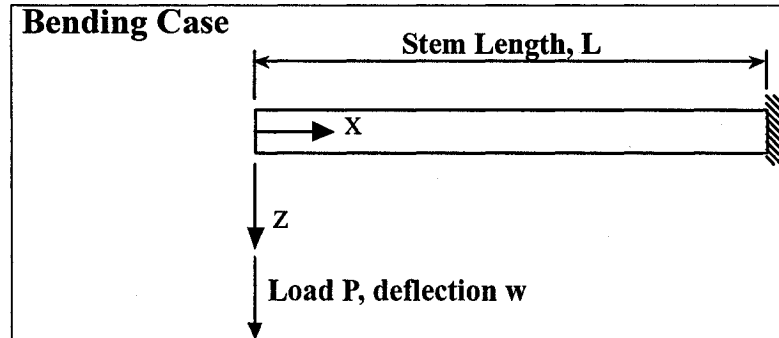


Figure 54: Simple case of clamped beam under bending load

From the values of load and deflection, the flexural stiffness ( $EI$ ) of the stem can be obtained from the following equation [99]:

$$EI = \frac{PL^3}{3w}$$

Equation 6: Bending stiffness of clamped beam under bending load

where:  $EI$  = Flexural stiffness  
 $P$  = Applied piston load  
 $w$  = Deflection at the load application point  
 $L$  = Length of cantilever beam (stem length)

The flexural stiffness is a value that can be used to compare one test to the other or to compare the current stem to competitor stems. Keep in mind that because the stem actually has a changing cross-section area, the value of  $EI$  represents an “average” value over the length of the stem.

### 8.3 Test Cases

#### Static pure torsion

The goal of this test is to determine the torsional rigidity (torsional stiffness) of the stem. Assuming small displacement theory, the measured displacement of the piston can be changed into a rotation angle  $\theta$  and plotted against torque (which is calculated from the applied load).

From the ISO specifications, the stem should be able to withstand a torque of at least 108 N-m. This value, converted for our lever arm, requires application of a piston load of 607 N on the assembly. The test peak load was set at 1000N, or approximately 178 N-m. The load was increased linearly, from 0 to 178 N-m, over a period of one minute, until it reached the peak value where it was kept for 15 seconds. Load was then released. The stem was tested for both the positive and negative directions of the piston, thus testing both positive and negative torsion modes.

#### Static bending

Similar to the static torsion test, the goal of the experiment is to find how stiff the stem is when a rider leans down on it (flexural stiffness). To verify this, the ISO norm requires no less than 1600 N applied at a 45-degree angle to the steerer axis. It was decided that the stiffness of the stem would be easier to compute if the load was applied directly in the steerer axis (see figure 4). The 1600 N-force applied at 45 degrees was transformed into components and the out-of-plane component, 1130 N was used. This gives essentially the same bending load as the ISO test. Since the control system always tends to undershoot, the peak load was set to 1150 N. The test was repeated a couple of times for each specimen. Once again, the load was increased linearly from 0 to 1150 N over a period of one minute and then

maintained at its peak for 15 seconds before being released. The load was only applied downwards as it represents the critical condition for this case.

### *Torsion fatigue*

The same torsion fixture was used to fatigue the stem body. The load was applied in a sinusoidal manner with set amplitude of 640 N, which converts to a torque of 114 N-m. During the cycle, the maximum load was 640 N and the minimum load was -640 N, thus the fatigue cycle went from the positive torsion to the negative torsion regimes (fully reversed fatigue loading). The ISO test recommended to apply two 200 N out of phase forces at each end of a chosen handlebar. Since the longest standard handlebar is approximately 47 cm wide, we converted the load value of 200 N to give an equivalent torque of 94 N-m (according to the dimensions and lever arms of the test apparatus). This way, the test load amplitude is set about 20% above the requirements, testing the part more intensively. The stem was twisted in both directions for 5,000 or 10,000 cycles, at a rate of one cycle every 4-seconds.

### *Bending fatigue*

The bending fatigue test was performed in both inward and outward directions, as prescribed by ISO. We applied a 950 N load amplitude with fully reversed loading (cycling from 950 N to -950 N) for 50000 cycles, using a rate of one cycle every 4-seconds. Fatigue testing uses the same fixture as the static test (shown in Figure 53). More cycles were performed in this test in comparison with the torsion fatigue since the FEA results showed an important zone of possible ply failure.

## 8.4 Tested Specimens

Unfortunately, although many specimens were built to test the process parameters and the resin, only few were available for testing. Therefore, it became important to get the most data out of each prototype. Table 7 presents the four tested specimens and the tests that were performed on each of them.

Name	Weight (g) Length (mm)	Resin	Lay-up	Tests (chronological order)
T1	114 120	Epon 862	Initial	Static Bending Static Torsion
T2	117 120	Derakane	Initial	Torsion Fatigue Static Torsion
T3	113 120	Miapoxy	Initial	Static Torsion Static Bending
T4	123 120	Miapoxy	Steerer tube reinforcement / larger braid diameter	Bending Fatigue Static Bending
ZOOM ALU	240 90	Comparative test - ALU		Static Bending Static Torsion
TRUATIV ROULEUR	145 120	Comparative test - ALU		Static Torsion Static Bending
TIME MONOLINK	132 120	Comparative test - Carbon		Static Torsion Static Bending
ALPHAQ BI-MATRIX	190 120	Comparative test - Carbon		Static Torsion Static Bending
ITM THE STEM	100 120	Comparative test - Magnesium		Static Torsion Static Bending
ITM MILLENium	165 120	Comparative test - Carbon		Static Torsion Static Bending
ITM UNIKO	165 90	Comparative test - Carbon		Static Torsion Static Bending

Table 7: Tested stems

Other tests were also performed on defective components (during product development) but the results are not included in this document.

## **8.5 Static Test Results**

All stems were statically tested in order to calculate stiffness values. Since it is not necessary to present every graph of the results of this section, only some typical examples will be presented in order to demonstrate the process and the type of raw data generated by the test machine's data acquisition system. The essential results will then be collated in a table at the end of the section.

### *Torsion stiffness*

As discussed previously, the collected data from the data acquisition unit are graphed and a regression is computed through the linear portion of the data. Since the static load ramps are applied several times on the same part, more than one set of results is obtained. An example is shown in Figure 55.

### Static Torsion Testing STEM T4

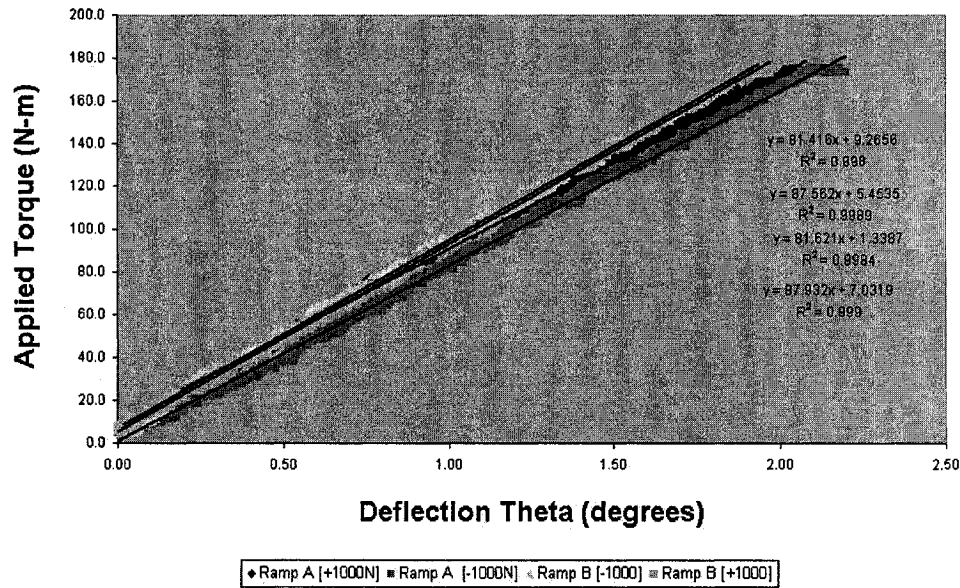


Figure 55: Static torsion test - Example of plotted results

The offset between the different ramps is due to the initial friction in the testing fixture. When the torsion on the stem is released, it is not always able to spring back completely, leaving the next test with a residual negative displacement. However this is not critical since the slope of the graph represents the real data of interest. In this graph, four stiffness values (representing two runs of the same test in positive torsion and two runs in negative torsion) are quite similar. Assuming that the rigidity in the positive and negative mode should be the same, average the four values is taken and only one scalar quantity for GJ is presented.

### Bending stiffness

Similarly to the torsion case, the displacements values collected are plotted against the applied load. Figure 56 is an example of a static bending test results.

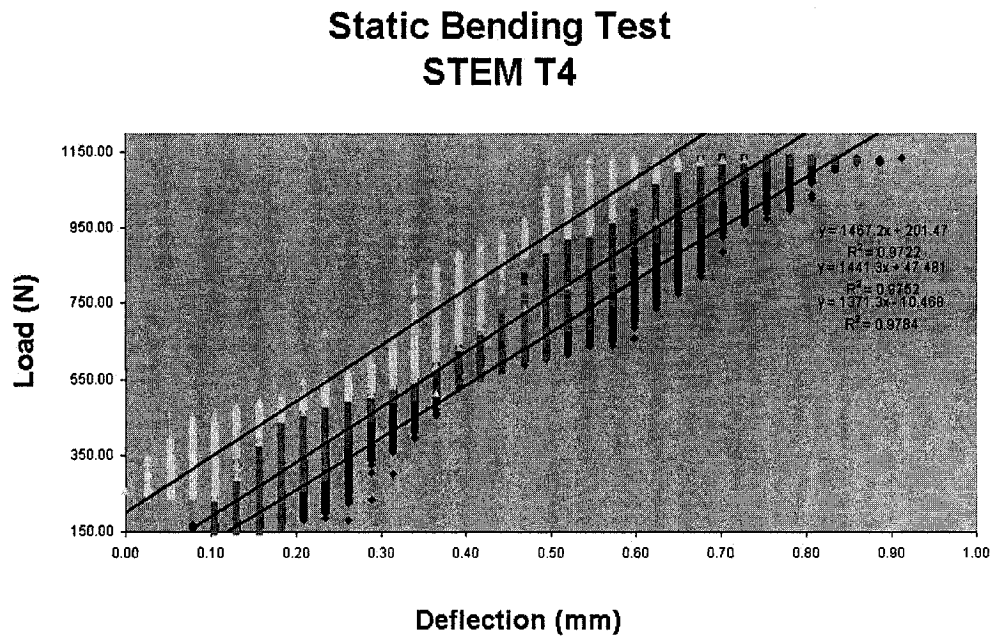


Figure 56: Static bending test - Example of plotted results

Note that each of the stems was tested at least a couple of times. Once again, the curve offsets are due to the restricted spring-back of the assembly after each test.



*Summary of static tests results*

Test Sample	Torsion Stiffness [GJ] (N-m <sup>2</sup> /radian)	Bending Stiffness [EI] (N-m <sup>2</sup> )
STEM T1	487	519
STEM T2	509	355
STEM T3	486	465
STEM T4	581	821

**Table 8: Static tests results for the different design iterations**

Table 8 shows that when loaded in pure torsion, the samples T1, T2 and T3 had very similar behavior. It is reasonable to assume the torsional rigidity of the initial lay-up to be around 490 N-m<sup>2</sup>. However, Stem T4 was found to be 20% stiffer in torsion, taking advantage of the minor lay-up changes that were introduced (the steerer tube reinforcement and the wider braid).

Although the differences between the design iterations did not seem to play a very important role in the torsion case, it greatly affected the bending stiffness. Essentially, this is explained by the exclusive use of +/- 45-degree braids in the construction. When a bending load is applied to the braided fibers, they tend to shear the resin, making the type of resin used and the complete wetting of the fibers more critical. This explains the large difference between T1 and T2, because T1 uses a higher quality resin. Unfortunately, as depicted in Section 5.1, this resin is very difficult to work with and it was not considered for production. Moreover, we can see that the new lay-up of T4 reaches almost twice the bending stiffness of the original stem. The new lay-up connecting the tube and the body fibers together provides a more integral structure resulting in improved stiffness properties. Moreover, the use of a

wider diameter braid changed the fiber orientation () and provided extra stiffness in the bending direction.

Test Sample	[GJ] (N-m <sup>2</sup> )	Specific [GJ] (N-m <sup>2</sup> ) / g	[EI] (N-m <sup>2</sup> )	Specific [EI] (N-m <sup>2</sup> ) / g
<b>STEM T4</b>	581	4.72	821	6.67
<b>Truativ ROULEUR</b>	540	3.72	522	3.60
<b>AlphaQ BI-MATRIX</b>	532	3.67	1290	6.79
<b>Time MONOLINK</b>	507	3.84	661	5.01
<b>ITM MILLENIUM</b>	506	3.07	1077	6.53
<b>ITM THE STEM</b>	316	3.16	780	7.80
<b>ITM UNIKO</b>	285	1.73	382	2.31
<b>Zoom ALU</b>	242	1.01	315	1.31

**Table 9: Stiffness properties of competitive products compared with the final design iteration**

When compared to other equivalent products in the industry, the stem shows very encouraging results. Table 9 presents a number of different competitor stem designs that were statically tested in order to get a performance measurement. It shows torsion and bending stiffness in columns 1 and 3, respectively. In addition GJ and EI are normalized with the weight of each stem (specific stiffness) shown in columns 2 and 4. An ideal stem would have high stiffness combined with low weight. Thus high values are expected in all columns. In cycling, stiffness is the main performance barometer as it indicates how much the component will twist or deflect under high loading (such as a sprint or a climb) [3]. In torsion, the latest prototype has surpassed competition by at least 10%. However, when taking the weight of each component into account (specific stiffness), T4 shows an undeniable advantage on all the other tested designs. As opposed to off-road cycling,

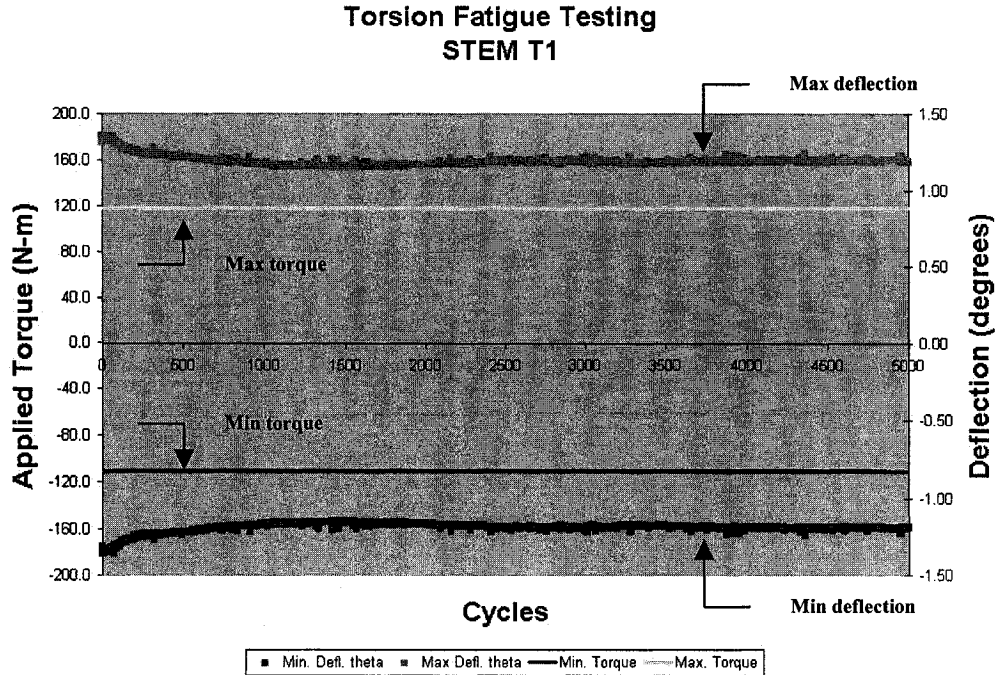
racers will appreciate a maximum of torsion stiffness in order to reduce the handlebar deflection to a minimum [100]. In bending, the stem showed slightly more compliance than some competitors. This is mainly due to the absence of unidirectional fibers. Still, compliance is sometimes judged as an advantage in road cycling since the extra flex on will act as a vibration damper and make the ride more comfortable [4]. We can also see that the specific bending stiffness is still quite high, proving that the designed shape takes full advantage of the material.

## 8.6 Fatigue Tests Results

Fatigue tests allow predicting the behavior of a mechanical part over time by applying a repetitive load for a set number of cycles. Once the tests are complete, another static test is usually conducted in order to verify if there is any decrease in static stiffness. Since fatigue tests normally decrease the mechanical properties of the parts, only one type of fatigue test was performed on each sample.

### Torsion fatigue

The T1 and T2 stems were subjected to 5000 and 10000 fully reversed cycles of 114 N-m respectively. The graph in Figure 57 shows the load applied and the corresponding extreme displacements. This way, we can interpret the changes in deflection due to damage caused by the repeated twisting. In a typical graph (like the one in Figure 57), two things are expected: a constant applied torque (because the test is being done in load control), and a relatively constant deflection reading until fatigue failure. At this point, the deflection will begin to increase slowly as a result of decreased stiffness. In Figure 57, since the deflection did not increase, failure did not happen.

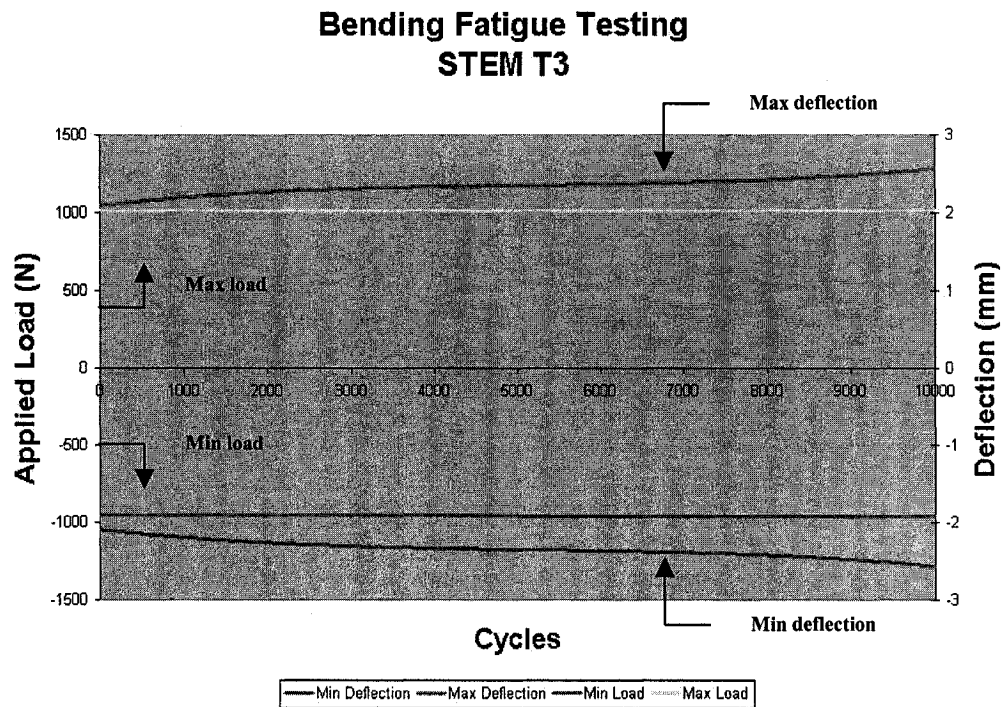


**Figure 57: Fatigue torsion test - Example of plotted results**

In Figure 57, an adaptation period can be seen, characteristic of the first few thousands of cycles. However, past 1700 cycles, the deflection remains constant, indicating no apparent fatigue damage.

### *Bending fatigue*

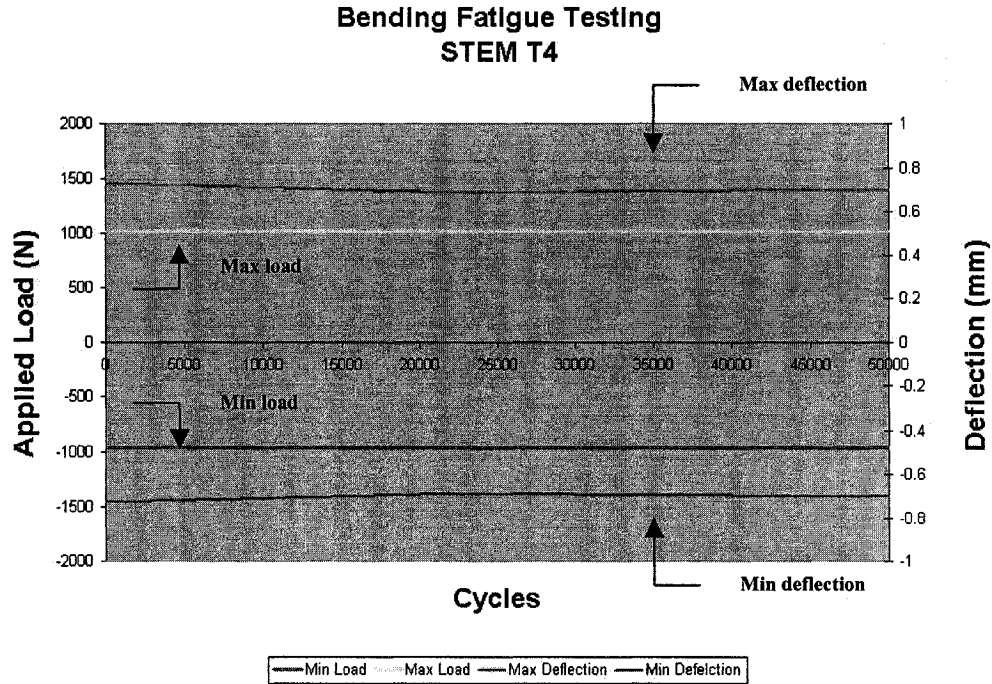
For bending fatigue of stem T3 (shown in Figure 58), a large and gradually increasing change in maximum deflection can be seen. This was mainly due to the early de-lamination of the steerer tube carbon insert from the rest of the stem body. From then onwards, the stem slowly continued failing by tearing the thin interface between the body and the tube insert, depicted by a gradually increasing deflection value (stiffness reduction).



**Figure 58: Bending fatigue failure results of stem T3**

Results from Figure 58 (and similar results) enabled the detection of a design flaw in the initial lay-up. Although it was not evident in the torsion test, it is clearly apparent in the bending test. The design of the carbon lay-up was changed, adding an interfacing carbon layer to the inside of the stem (described in section 2.3 and Figure 13). This way, the tube insert would no longer be connected to the body solely by its rim, but by an overlapping carbon fiber layer that forms a lap joint between the tube and the stem body (Figure 13-B).

Stem T4 was subjected fatigue testing for 50,000 cycles and showed an impressive change in reliability when compared to the other samples. Since the tube did not delaminate, it allowed the stem to keep its rigidity throughout the entire process. The results are shown in Figure 59.



**Figure 59: Bending fatigue of sample T4**

*Summary of fatigue results*

Sample	Torsional Rigidity [GJ] (N-m <sup>2</sup> )			Bending Rigidity [EI] (N-m <sup>2</sup> )		
	Initial	After Conditioning	After Fatigue	Initial	After Conditioning	After Fatigue
STEM T1	487	555	539	519		
STEM T2	509	542	511	355		
STEM T3	486			465	Gradual damage	374
STEM T4	581			821	855	855

**Table 10: Fatigue tests results**

The collected results show that the torsion fatigue was not a problem in the initial design. The two tests showed no decrease in torsion stiffness after the repeated loading. Stem T1 even shows an increase in torsional stiffness.

This apparent discrepancy is not unusual in the field of composite structures. When a composite structure is subjected to low level fatigue loading, the fibers will initially tend to stretch and settle themselves in a better way to counter the load. This is sometimes called the “conditioning period”. Because of this phenomenon, the stiffness can increase slightly. This phenomenon has been described in previous research, as seen in Figure 60 below. The figure clearly shows that when a unidirectional carbon sample is fatigue tested in tension, it will appear to have an increase in stiffness in the early portion of the cycling.

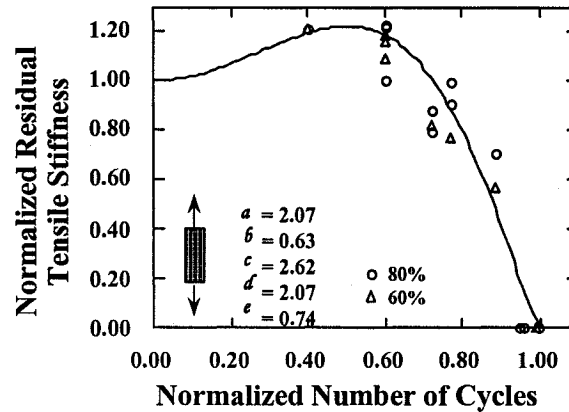


Figure 60: Normalized residual stiffness of a unidirectional 0° ply under longitudinal tensile fatigue loading conditions [101]

Note that the increase can be relatively large (almost 20%) for residual stiffness in the fiber direction. This phenomenon is the reason why some samples have increased rigidity after fatigue testing (see Table 10). The stems are being subjected to relatively low-level fatigue resulting in minimal damage and “stiffness conditioning”.

However, the precarious bonding joint between the steerer tube and the rest of the stem revealed an important design weakness in the fatigue bending tests. The stiffness value of T3 after fatigue is greatly reduced. However, the design problems were solved in the final version of the stem

(T4). It showed minimal change in deflection after 50,000 cycles and even gained some bending rigidity after the conditioning period.

Inspecting the results of these tests, it is believed that it is a good idea to condition the samples for a few thousand cycles before testing the initial stiffness. Although it does not have any negative effect on the final product, it would be easier to compare the change in rigidity after fatigue loading.

An ultimate bending load test was attempted in order to see when the stem would break. However, the equipment reached the piston load limit of 3000 N without breaking the stem in bending. Once again, this is a very positive result that ensures that the clamping method and the body construction is adequate and will not fail, even under extreme loading.



## 9. CONCLUSIONS

The scope of this research was the complete design process of a carbon fiber bicycle stem. All aspects of the design were successful, beginning with a final part weight of 123 g. Moreover, use of carbon fiber over metallic inserts was maximized with less than 2% of the structural weight was in metallic inserts (excluding fasteners). The concurrent design and mechanical analysis helped to design a shape minimizing stress concentrations. From the model, a complete set of molds was manufactured and several prototypes were produced. Experiments allowed debugging of the manufacturing method and evaluating different resin systems. Flow simulation models proved particularly useful at identifying the source of recurring defects and evaluating solutions.

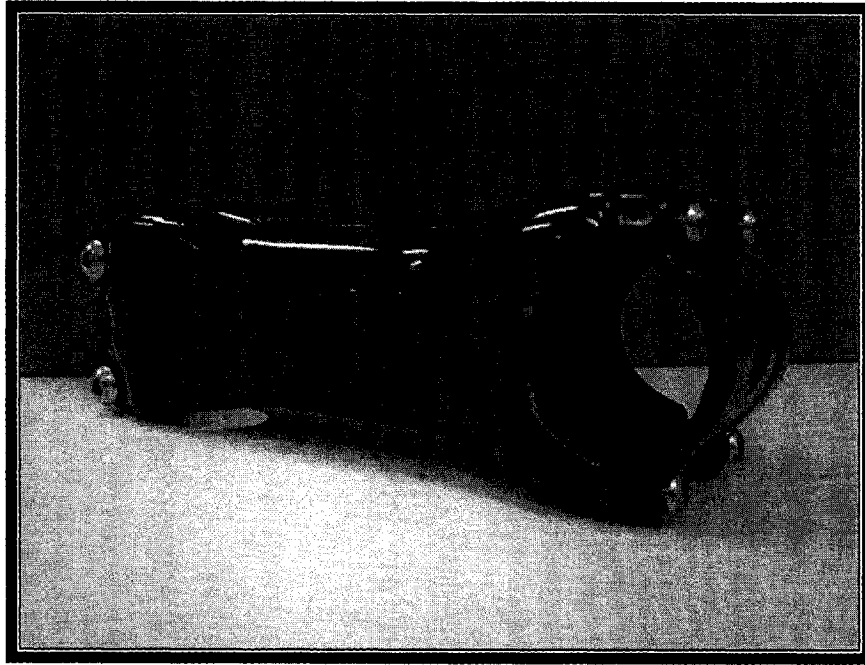
The combined molding using RTM and an inflatable core presented difficulties but proved to be the most efficient process for this application. The development of a multi-purpose bladder holder allowed the part to come out of the mold without any further bonding required. This demonstrates the part integration capabilities of the RTM process. The need for removal of the extra material led to the design of post-injection machining fixtures that allowed for repeatability in the production of prototypes.

These prototypes were used to perform tests and find an important flaw in the design that was solved by adding extra reinforcement in the lay-up. The modifications showed significantly improved behavior in both torsion and in bending. Comparative tests placed the stem above all the competition in all measured categories with an impressive stiffness to weight ratio.

One of the main contribution of this thesis lies in the development of manufacturing methods for composite materials, specifically in the area of RTM processing.

This research shows an opportunity to further optimize fiber reinforced hollow components. The design of the manufacturing system shows how it is possible to use the inner bladder/RTM molding method, even when the part is

relatively small and complex in terms of shape and inserts. Thus, the method shows great potential for use in other industries such as aerospace or automotive.



**Figure 61: The final product**

## 10. REFERENCES

1. **Prince, K.** "Composites win over sports market." *Reinforced Plastics*, **46/ 9** (2002), 48-51.
2. **Takada, N.** "Progress in sport goods and technologies for applying advanced composite materials to sport goods." *International SAMPE Symposium and Exhibition (Proceedings)*, **41/1** (1996), 393-404.
3. **Nelson, R.**, "Bike frame races carbon consumer goods forward." *Reinforced Plastics*, **47/7** (2003), 36-40.
4. **Ziegmann, G.** and **M. Hintermann.** "Fibre composite mountain bike. Example of a strategy for the development of highly integrated structures." *Kunststoffe Plast Europe*, **89/2** (1999), 31-34.
5. **Spencer, B. E.** "Composites in the sporting goods industry." *Handbook of composites*. S.T. Peters Ed., Chapman & Hall, London, 1998, 1044-1052.
6. "Peddling a £4000 dream. Advanced composites for pedal bikes." *Professional Engineering*, **10/4** (1997), 34.
7. **Levin, S.C.** "Composites and bicycles: Market diversification in action." *International SAMPE Symposium and Exhibition (Proceedings)*, **38/2** (1993), 1470-1482.
8. **Lessard, L., J. Nemes** and **P. Lizotte**, "Utilization of FEA in the design of composite bicycle frames." *Composites*, **26/1** (1995), 72-74.
9. **Lizotte, P.** *Stress analysis and fabrication of composite monocoque bicycle frames*. M.Eng Thesis, McGill University, 1996.
10. **Giant Bicycle.** *Home Page*. [<http://www.giant-bicycle.com/cn>] – 2004.
11. **Jones, C.** *Bicycle headset standards and nomenclature*. [[http://www.parktool.com/repair\\_help/howfix\\_headtypes.shtml](http://www.parktool.com/repair_help/howfix_headtypes.shtml)] – 2004.
12. **Cane Creek.** *The Aheadset*. [<http://www.canecreek.com/site/product/headset/index.html>] – 2004.
13. **Cane Creek.** *Aheadset*. [<http://www.canecreek.com>] – 2001.
14. **ITM.** *Home Page*. [<http://www.itm.it>] – 2004.
15. **Titec.** *Home Page*. [<http://www.titec.com>] – 2004.
16. **Jenson USA.** *Thomson Elite Road Stem*. [<http://www.jensonusa.com/store/product.aspx?i=ST707B00>] – 2004.
17. **Time.** *Home Page*. [<http://www.timesportusa.com>] – 2004.
18. **3TTT.** *Home Page*. [<http://www.3ttt.com>] – 2004.
19. **Deda Elementi.** *Home Page*. [<http://www.dedaelementi.com>] – 2004.
20. **Berthelot, J.-M.** *Composite Materials – Mechanical behavior and structural analysis*, Springer, New York, 1999, 3.

21. **Potter, K.** *Resin transfer molding*, Chapman & Hall, UK, 1997, pp. 28-37, 62-69, 146-149, 186.
22. **Matthews F.L. and R.D. Rawlings.** *Composite materials: Engineering and science*, CRC Press, Woodhead Publishing limited, Cambridge, 1999, 184.
23. **Lai, G.** "Inside project '96'." *Bicycle Guide Magazine*, July 1996, 34-37.
24. **Kestrel USA.** *Newsroom: Ultra light Carbon Fibre/Epoxy Road Bike.*  
[<http://www.netcomposites.com/news.asp?2072>] – 2004
25. "Developments in resin transfer moulding." (Authors name not provided by journal), *Reinforced Plastics*, 35/6 (June 1991), 34-37.
26. **Potter, K.D.** "The early history of the resin transfer moulding process for aerospace applications." *Composites Part A*, 30/5 (May 1999), 619-621.
27. **Fong, L. and S.G. Advani.** "Resin transfer molding." *Handbook of composites*. S.T. Peters Ed., Chapman & Hall, London, 1998, 433-455.
28. "Fiesta's RTM spoiler breaks new ground." (Authors name not provided by journal), *Reinforced Plastics*, March 1996, 20-24.
29. **Ludik, J.** "Resin transfer moulding for missile shroud production." *ICCM-11 (proceedings)*, Gold Coast, Australia, 14<sup>th</sup>-18<sup>th</sup> July 1997, Book IV, 55-63.
30. "Closed mold processing." *Reinforced Plastics*, February 2001, 28-34.
31. **Strong, B.** *Fundamentals of composite manufacturing: Materials, methods and applications*, Society of Manufacturing Engineers, Dearborn, 1989.
32. **Lehmann, U. and W. Michaeli.** "Combined moulding speeds hollow parts", *Reinforced Plastics*, 40/3 (1996), 40-43.
33. **Mccaffery, T. R., Z.Z. Zguris and Y. G. Durant.** "Low cost mold development for prototype parts produced by vacuum assisted resin transfer molding (VARTM)." *Journal of Composite Materials*, 37/10 (2003), 899-912.
34. **Shih, C.-H. and L.J. Lee.** "Tackification of textile fiber preforms in resin transfer molding." *Journal of Composite Materials*, 35/21, 2001, 1954-1981.
35. **Berthet, F., P. Devos and T. Ansart,** "Demonstrating the need of taking into account the compatibility tackifier/resin, and processing conditions to control mechanical properties of RTM CFRP." *Annual Technical Conference - ANTEC, Conference Proceedings*, 2 (1997), 2377-2381.
36. **Trochu, F., R. Gauvin and D.-M. Gao.** "Numerical analysis of the resin transfer molding process by the finite element method." *Advances in Polymer technology*, 12/4 (1993), 329-342.
37. **Gauvin, R., F. Trochu, Y. Lemenn and L. Diallo.** "Permeability measurement and flow simulation through fiber reinforcement." *Polymer Composites*, 17/1 (1996), 34-42.

38. **Octeau, M.-A. and L. Lessard.** "Design of a lightweight composite bicycle fork." *Cancom 2001: Third Canadian International Composites Conference*, Quebec, Canada, 21-24 Aug. 2001. 2001-2007.
39. **M. Quaresimin, G. Meneghetti and F. Verardo.** "Design and optimisation of an RTM composite bicycle crank." *Journal of Reinforced Plastics and Composites*. **20/2** (2001), 129-146.
40. **Lane, D.M., J.J. Kutz, S.D. DeRoos, and K.R. Alesse.** "Comparison of processing techniques for the molding of hollow advanced composite parts." *Proceedings of the 38th International SAMPE Symposium and Exhibition*, **38/1** (1993), 522-532.
41. **Juang, B.** "Research and development of composite sporting goods in Marshal." *International SAMPE Symposium and Exhibition (Proceedings)*, **41/1** (1996), 379-392.
42. **Lehmann, U. and W. Michaeli.** "Preforming of fiber reinforced hollow components with the RTM /bladder molding process." *Advanced composites; Proceedings of the 9th Annual ACCE Conference*, **9** (1997), 531-541.
43. **Dreschler, K.** "3D- textile reinforced composites for the transportation industry." *3-D textile reinforcements in composite materials*, A. Miravete Ed., CRC Press, Woodhead Publishing limited, Cambridge, 1999, 43-66.
44. "Composite baseball bats with striking features." *Reinforced Plastics*, September 2002, 52-55.
45. **Lehmann, U. and W. Michaeli.** "Cores lead to an automated production of hollow composite parts in resin transfer moulding." *Composites Part A*, **29/7**, 1998, 803-810.
46. **Lehmann, U. and W. Michaeli.** "Improved processing of resin transfer molding for the production of hollow parts with inflatable bladders." *Proceedings of the 42nd International SAMPE Symposium and Exhibition*, **42/1** (1997), 13-23.
47. **A&P Technology Inc.** *The Braid Calculator* [<http://www.braider.com>] – 2004.
48. **Michaeli, W., J. Dyckhoff and M. Jehrke.** "Production of structural hollow fibre reinforced components using a combined RTM and blow-up technology." *Proceedings of the 38th International SAMPE Symposium and Exhibition*, **38/2** (1993), 2092-2101.
49. **Zinn, L.** *How many bolts*, [<http://www.insidetri.com/train/bike/articles/1862.0.html>] – 2004.
50. **A&P Technology Inc.** *Standard Products – Gammasox*. [<http://www.braider.com>] – 2004.
51. **Nadari, C., B. Ferret and D. Gay.** "Simultaneous engineering in design and manufacture using the RTM process." *Composites: Part A*, **33** (2002), 191-196.

52. **ASTM D4762 (D3039/D3039M)**, "Standard guide for testing polymer matrix composite materials", ASTM International, 2004.
53. **Hashin, Z., D. Bagchi and W. Rosen.** "Non-linear behavior of fiber composite laminates." *NASA Contractor Report 2313*, National Aeronautics and Space Administration, 1974.
54. **Jones, R. M. and H. S. Morgan.** "Analysis of nonlinear stress-strain behavior of fiber reinforced composite materials". *AIAA Journal*, **15/12** (1997), 1669-1676.
55. **Golubovic, A. and L. Lessard.** "Analysis and optimization of adhesively bonded joints." *ECCM/9, European Conference on Composite Materials (Proceedings)*, Brighton, England, June 4-7, 2000, CD ROM.
56. **Van der Aa, H.C.E.** *Re-design and manufacturing of a composite monocoque bicycle frame*. Joint Technical Report, McGill University and T.U. Eindhoven, Netherlands, 1997.
57. "Tooling for RTM." (Authors name not provided by journal), *Reinforced Plastics*, **35/6** (June 1991), 20-23.
58. **Campbell, F.C.** *Manufacturing processes for composite materials*, Elsevier, Oxford, 2004, 326-338.
59. **Huntsman/RenShape solutions.** *Ren 6430 Product Data*, [<http://www.huntsman.com/renshape>] – 2004.
60. **Clifford, M. and A. Long.** "Flow characterization for partially impregnated prepregs." *ECCM 11 (Proceedings)*, Rhodes, Greece, May 31<sup>st</sup> – June 3<sup>rd</sup>, 2004 CD ROM.
61. **Payan, S., Y. Le Petitcorps, J.-M.Olive and H. Saadaoui.** "Experimental procedure to analyse the corrosion mechanisms at the carbon/aluminum interface in composite materials." *Composites - Part A*, **32/3** (2001), 585-600.
62. **Golubovic, A..** *Analysis and optimization of adhesively bonded joints*, M.Eng.Thesis, McGill University, March 2000.
63. **Ferret, B., M. Anduze and C. Nardari.** "Metal inserts in structural composite materials manufactured by RTM", *Composites Part A*, **29** (1998), 693-700.
64. **Octeau, M.-A.** *Composite bicycle fork design for vacuum assisted resin transfer Moulding*, M.Eng. Thesis, McGill University, August 2001.
65. **BigHead Bonding Fasteners.** *Homepage*. [<http://www.bighead.co.uk>] – 2004.
66. **Rotaloc International.** *Homepage*. [<http://www.rotaloc.com/>] – 2004.
67. **Tucker, W. C., R. Brown and L. Russell.** "Corrosion between a graphite/polymer composite and metals", *Journal of composite materials*, **24** (1990), 92-102.
68. **Latex Technology.** *Homepage*. [<http://www.latextechnology.com/>] – 2004.
69. **EMC Squared.** *Products*. [<http://www.emcsquared.com/products.html>] – 2004.

70. **Michael Engineering Ltd.** *Homepage*. [<http://www.michaelengineering.com>] – 2004.
71. **Radius Engineering.** *2100 p - Spec. Sheet*. [<http://www.radiuseng.com/2100p.pdf>] – 2004.
72. **Rudd, C.D., A.C. Long, K.N. Kendall and C.G.E. Mangin.** *Liquid moulding technologies*, Woodhead Publishing limited, Cambridge, 1997, 65-97.
73. **McMaster-Carr Industrial Supplies.** *Tubing* [<http://www.mcmaster.com>] – 2004.
74. **Dow Chemicals.** *Derakane 8084 - Technical data sheet*, provided by Progress plastics, 2003.
75. **Resolution Performance Products.** *Starting formulation 8025 - Data sheet*, [<http://www.resins.com/resins/am/pdf/SC2508.pdf>], 2003.
76. **Resolution Performance Products.** *Starting formulation 8022 - Data sheet*, [<http://www.resins.com/resins/am/pdf/SC1183.pdf>], 2003.
77. **M F Composites.** *Miapoxy 100 H 90 - Technical data sheet*, 2003.
78. **Liu, C.J., M.S. Kiasat, A.H.J. Nijhof, H. Blokland and R. Marissen.** "Effect of the addition of a low profile additive on the curing shrinkage of an unsaturated polyester resin." *Polymer Engineering and Science*, **39/1** (Jan 1999), 18-25.
79. **Kinkelaar, M., B. Wang and L. J. Lee.** "Shrinkage behaviour of low-profile unsaturated polyester resins." *Polymer*, **35/14** (July 1994), 3011-3022.
80. "Bicycle frame uses combination RTM/blow-moulding process." (Authors name not provided by journal), *Advanced Composites Bulletin*, 1994, 4-5.
81. **Jinlian, H, L. Yi and S. Xueming.** "Study on void formation in multi-layer woven fabric." *Composites Part A*, **35/5** (2004), 595-603.
82. **Guyot, H..** "La simulation de procedes relance le RTM, industries et techniques." n. 817 (2000), 55-57.
83. **El Hadj, M. et S. Burg.** "Simulation du remplissage d'un moule en RTM." *Plastiques Modernes et Elastomeres*, **50/3** (1998), 22-25.
84. **Baichen, L., S. Bickerton and S.G. Advani.** "Modeling and simulation of resin transfer moulding (RTM) – gate control, venting and dry spot prediction." *Composites: Part A*, **27** (1996), 135-141.
85. **Advani, S. G. and Dr. D. Heider.** "Role of mold filling simulations in composite Manufacturing." Invited Speaker, *11<sup>th</sup> European Conference on Composite Materials (ECCM 11)*, May 31<sup>st</sup> – June 3<sup>rd</sup>, Rhodos, Greece.
86. **Hsiao, K.-T., J.W. Gillespie Jr. and S.G. Advani.** "Role of vacuum pressure and port location on flow control for liquid composite molding processes." *Polymer Composites*, **22/5** (2001) 660-667.

87. **Um, M.K., B.-H. Kim, B.S. Kim and E.-J. Jun.** "A development of composite Artificial Leg Shell Using RTM Process." *ICCM-11 (proceedings)*, Gold Coast, Australia, 14<sup>th</sup>-18<sup>th</sup> July 1997, Book I, 477-487.
88. **Pantelidis, N.G.** "A low-cost composite bicycle frame produced by RTM: From concept to reality." *Annual Technical Conference - ANTEC, Conference Proceedings*, May 4-8, Nashville, TN, United States, **2** (2003), 2054-2058.
89. **Yoon, M.K., P. Barooah, B. Berker and J.Q. Sun.** "Permeability and porosity estimation in resin transfer molding", *Journal of Materials Processing & Manufacturing Science*, **7** (1998), 173-184.
90. **Ruiz, E. and F. Trochu.** *Guidelines for the preparation of test samples for pre-form permeability measurements*. Department of Mechanical Engineering, École Polytechnique de Montréal, Montréal, 2001.
91. **ESI Software.** *PAM-RTM 2002 User's documentation*. August 2002.
92. **Rahman, M., S. Ramakrishna, J.R.S. Prakash and D.C.G. Tan.** "Machinability study of carbon fiber reinforced composite." *Journal of Materials Processing Technology*, **89-90** (1999), 292-297.
93. **Lin, S.C. and I.K. Chen.** "Drilling carbon fiber-reinforced composite material at high speed." *Wear*, **194/1-2** (1996), 156-162.
94. **Chen, W.-C.** "Some experimental investigations in the drilling of carbon fiber-reinforced plastic (CFRP) composite laminates." *International Journal of Machine Tools & Manufacture*, **37/8** (1997), 1097-1108.
95. **Won, M.S. and C.K.H. Dharan.** "Drilling of aramid and carbon fiber polymer composites." *Journal of Manufacturing Science and Engineering, Transactions of the ASME*, **124/4** (2002), 778-783.
96. **Hailand, C.J.** "Diamond coated tools to tackle composites." *Metal Powder Report*, **53/10** (1998), p.16.
97. **Larson, M.** "Composites make the leap from bombers to bike." *Quality*, **37/9** (1998), 30-35.
98. "ISO 4210" (1996), rev. 2001-08-15.
99. **Beer, F.P. and E.R. Johnston,** *Mechanics of materials - Second Edition*, McGraw-Hill, England, 1992, pp. 129, 716
100. **Fried, J.** "Design and development of a composite monocoque airfoil road racing bicycle frame." *SAMPE Journal*, **34/4** (1998), 46-50.
101. **Lessard, L. and M. Shokrieh.** "Fatigue of composites" Chapter 3 on "Multiaxial Fatigue." B. Harris Ed., Woodhead Publishing, Cambridge, 2003.
102. **Tovo, R.** "On the fatigue reliability evaluation of structural components under service loading." *International Journal of Fatigue*, **23/7** (2001), 587-598.